Electronic Supplementary Material (ESI) for Physical Chemistry Chemical Physics.


# Computational study on the reactivity of imidazolium-functionalized manganese bipyridyl tricarbonyl electrocatalysts $[Mn[bpyMe(Im\text{-}R)](CO)_3Br]^+$ (R = Me, $Me_2$ and $Me_4$) for $CO_2$-to-CO conversion over $H_2$ formation

Xiaohui Li and Julien A. Panetier*

Department of Chemistry, State University of New York at Binghamton, Binghamton, New York, 13902, USA. E-mail: panetier@binghamton.edu

*-Supporting Information-*

**Table of Contents**

**1. Additional computational details.**

All reported redox potentials were calculated using the direct approach in which the Gibbs free energies of the reactants, intermediates and products were calculated directly in acetonitrile using the SMD approach, rather than by a thermodynamic cycle involving gas-phase energies.[1] All potentials reported herein (in V) are versus the $Fc^{+/0}$ redox couple and were obtained using the following expressions:

$$A + Fc \leftrightharpoons A^- + Fc^+ \quad (1)$$

$$\Delta G^*_{red,soln} = G^*_{red,soln}(A^-) + G^*_{red,soln}(Fc^+) - G^*_{red,soln}(A) - G^*_{red,soln}(Fc) \quad (2)$$

$$E^0 = -\frac{\Delta G^*_{red,soln}}{nF} \quad (3)$$

where the "$*$" superscripts denote that the quantities were computed at a standard state of 1 M. In Equation 2, $G^*_{red,soln}(A^-)$ represents the Gibbs free energy in solution of the one-electron reduced species, $G^*_{red,soln}(Fc^+)$ is the Gibbs free energy in solution of ferrocenium, $G^*_{red,soln}(A)$ corresponds to the Gibbs free energy in solution of the non-reduced species, and $G^*_{red,soln}(Fc)$ is the Gibbs free energy in solution of ferrocene. Based on the Gibbs free energy change, the reduction potentials were calculated according to Equation 3 where $n$ is the number of electron(s) involved in the process (in this case, $n = 1$ for a one-electron process) and $F$ is the Faraday constant.

All energies were corrected for zero-point vibrational energy, while free energies (quoted at 298.15 K and 1 atm) were corrected using the modified harmonic oscillator approximation proposed by Grimme where low-lying vibrational modes were treated by a free-rotor approximation.[2] An applied potential of $\Phi$ = -1.82 V versus the $Fc^{0/+}$ couple was employed to model each electrochemical step, which corresponds to the applied potential of the controlled potential electrolysis (CPE) experiments.[3] Finally, natural bond orbital (NBO) analyses were performed with NBO version 3.1,[4] as implemented in Gaussian 09.[5]

## 2. Computational data.

To investigate how the substituents at the C2 and C4/C5 positions on the imidazolium moiety affect catalysis for the $CO_2$ reduction reaction ($CO_2$RR), we explicitly considered six different configurations: $\mathbf{1}_{\mathbf{C2}}^{+}$, $\mathbf{1}_{\mathbf{C5}}^{+}$, $\mathbf{2}_{\mathbf{C2}}^{+}$, $\mathbf{2}_{\mathbf{C5}}^{+}$, $\mathbf{3}_{\mathbf{C2}}^{+}$ and $\mathbf{3}_{\mathbf{C5}}^{+}$ (Figure S1). The computed Gibbs free energy profiles for $\mathbf{1}_{\mathbf{C2}}^{+}$ is discussed in the main text, while the calculated Gibbs free energy profiles for the other five catalysts are described in the supporting information.

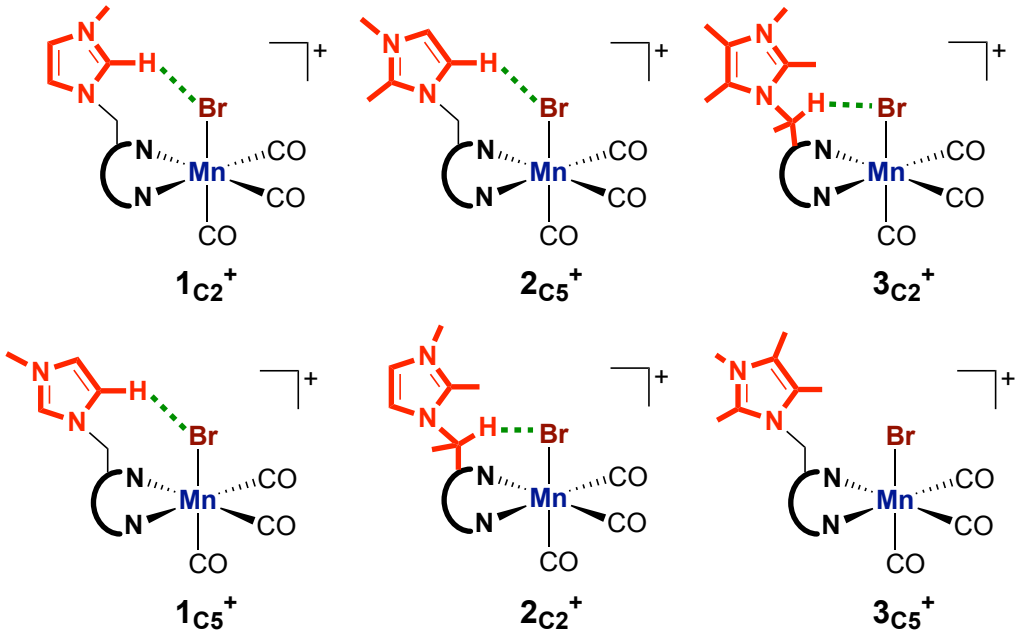


**Figure S1.** Schematic representation of the six imidazolium-functionalized manganese bipyridyl tricarbonyl electrocatalysts that have been investigated in this work. In the case of $\mathbf{2}_{\mathbf{C2}}^{+}$ and $\mathbf{3}_{\mathbf{C2}}^{+}$, the lowest energy structures feature a hydrogen-bonding interaction between the methylene bridge and bromide.[3]

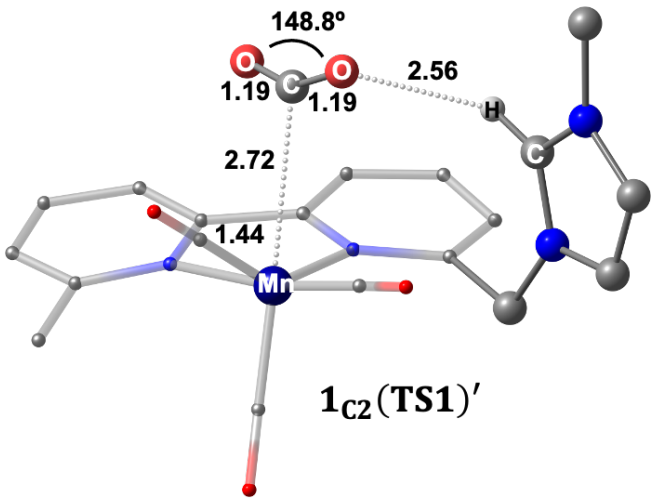


**Figure S2.** Optimized geometries of the transition state $\mathbf{1_{C2}(TS1)'}$ for the formation of the metallocarboxylate intermediate in which the imidazolium ligand weakly interacts with $CO_2$ instead of cooperating with the axial carbonyl ligand (Figure 4). This transition state, which has an open-shell singlet ground-state ($\rho_{Mn} = 0.26$; $\langle S^2 \rangle = 0.13$), is 1.1 kcal/mol higher in energy than $\mathbf{1_{C2}(TS1)}$. Distances are given in angstroms, and the bond angle is in degree. Non-participating hydrogen atoms are omitted for clarity.

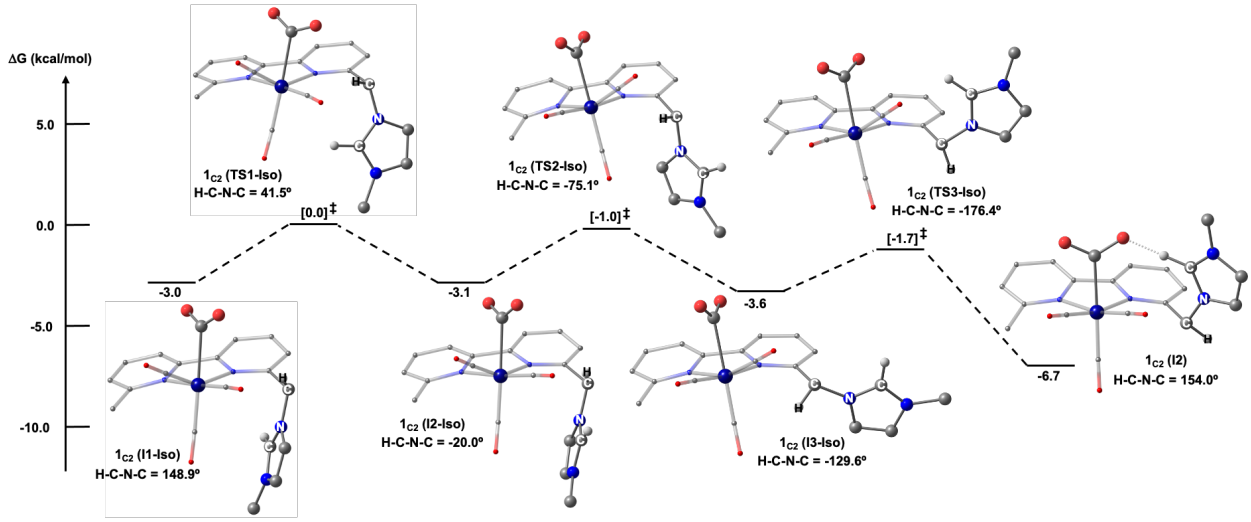


**Figure S3.** Computed free energy (kcal/mol) profile for the isomerization of the Mn-$CO_2$ adduct in which the imidazolium ligand initially interacts with the axial carbonyl ligand before cooperating with the $CO_2$ moiety. All free energies are calculated with respect to the separated reactants.

**2.1. Formation of the metallocarboxylic acid intermediates $\mathbf{2}^{+}_{\mathbf{C5}}(\mathbf{I5})$ and $\mathbf{3}^{+}_{\mathbf{C2}}(\mathbf{I5})$.** To understand the effect of the substituents on the imidazolium ligand, the Gibbs free energy reaction profiles for [Mn[bpyMe(ImMe$_2$)](CO)$_3$Br]$^+$ (**2**$^+$) and [Mn[bpyMe(ImMe$_4$)](CO)$_3$Br]$^+$ (**3**$^+$) were computed and compared with the calculated free energy profile for **1**$^+$.

Similar to yielding the metallocarboxylic acid intermediate $\mathbf{1}^{+}_{\mathbf{C2}}(\mathbf{I5})$, the initial formation of the doubly reduced complexes $\mathbf{2}_{\mathbf{C5}}(\mathbf{red2})$ and $\mathbf{3}_{\mathbf{C2}}(\mathbf{red2})$ is required to activate $CO_2$, and yield, respectively, the Mn-$CO_2$ adduct species $\mathbf{2}_{\mathbf{C5}}(\mathbf{I2})$ and $\mathbf{3}_{\mathbf{C2}}(\mathbf{I2})$ (Figures S4 and S5). As seen for **1**$^+$, the computed transition states for $CO_2$ binding $\mathbf{2}_{\mathbf{C5}}(\mathbf{TS1})$ shows that the imidazolium ligand interacts with the carbonyl ligand rather than with $CO_2$ (Figure S6). In contrast, the lowest energy transition state for the third catalyst reveals that the imidazolium group cooperates with $CO_2$, suggesting a direct implication of the functional groups in the secondary coordination sphere for yielding the metallocarboxylate species (Figure S6).

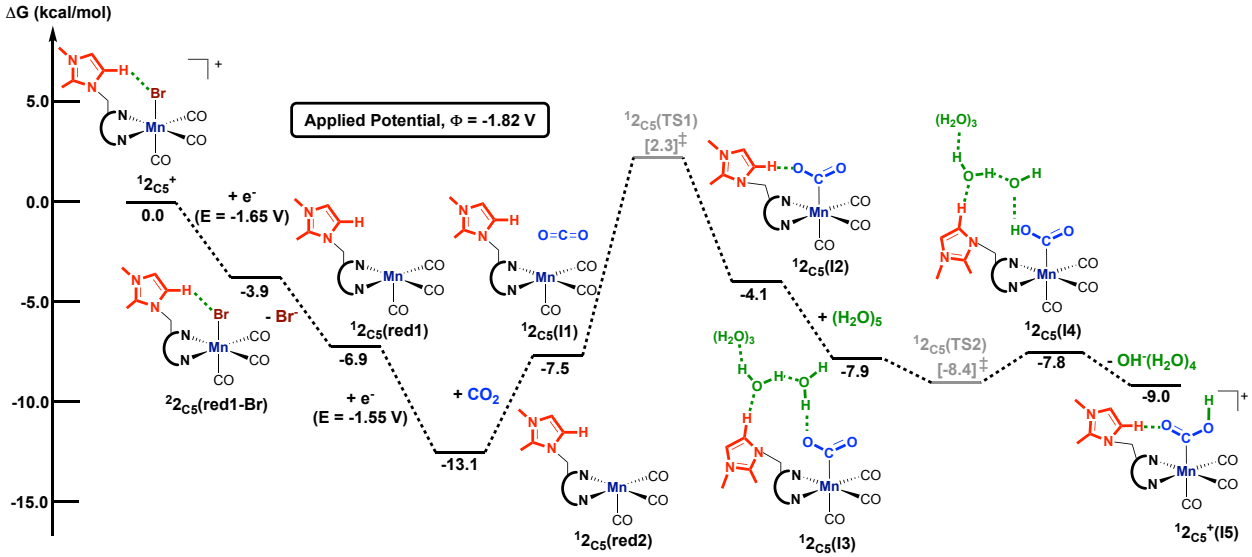


**Figure S4**. Computed free energy (kcal/mol) profile for the formation of the metallocarboxylic acid species, $\mathbf{2}^{+}_{\mathbf{C5}}(\mathbf{I5})$. All free energies are calculated with respect to the separated reactants and the superscript corresponds to the spin multiplicity of a given species. The computed electronic energy for $\mathbf{2}_{\mathbf{C5}}(\mathbf{TS2})$ is higher than that of $\mathbf{2}_{\mathbf{C5}}(\mathbf{I3})$ and $\mathbf{2}_{\mathbf{C5}}(\mathbf{I4})$. However, $\mathbf{2}_{\mathbf{C5}}(\mathbf{TS2})$ has a lower zero-point energy than both intermediates, offsetting its higher Gibbs free energy.

As seen for **1**$^+$, the optimized Mn-$CO_2$ adducts in **2**$^+$ and **3**$^+$ have a closed-shell singlet ground-state, featuring two electrons on $CO_2$ along with a Mulliken spin population on the manganese of zero. For instance, the optimized geometry of $\mathbf{2}_{\mathbf{C5}}(\mathbf{I2})$ shows an O=C=O angle of 126.1° and a

$C_{py}$–$C_{py}$ bond length of 1.48 Å on the bipyridine ligand, revealing the formation of a carboxyl group (Figure S7). Furthermore, species $\mathbf{2_{C5}(I2)}$ and $\mathbf{3_{C2}(I2)}$ show similar geometries with $\mathbf{1_{C2}(I2)}$ in which the imidazolium moiety interacts with the carboxyl group via hydrogen-bonding interactions. Overall, the computed Gibbs free energies for the Mn-$CO_2$ adducts follow the expected trend: $\mathbf{1_{C2}(I2)}$ ($\Delta$G = -6.7 kcal/mol with respect to the separated reactants) < $\mathbf{2_{C5}(I2)}$ ($\Delta$G = -4.1 kcal/mol) = $\mathbf{3_{C2}(I2)}$ ($\Delta$G = -4.1 kcal/mol), further revealing that the imidazolium ligand in the secondary coordination stabilizes the metallocarboxylate species.

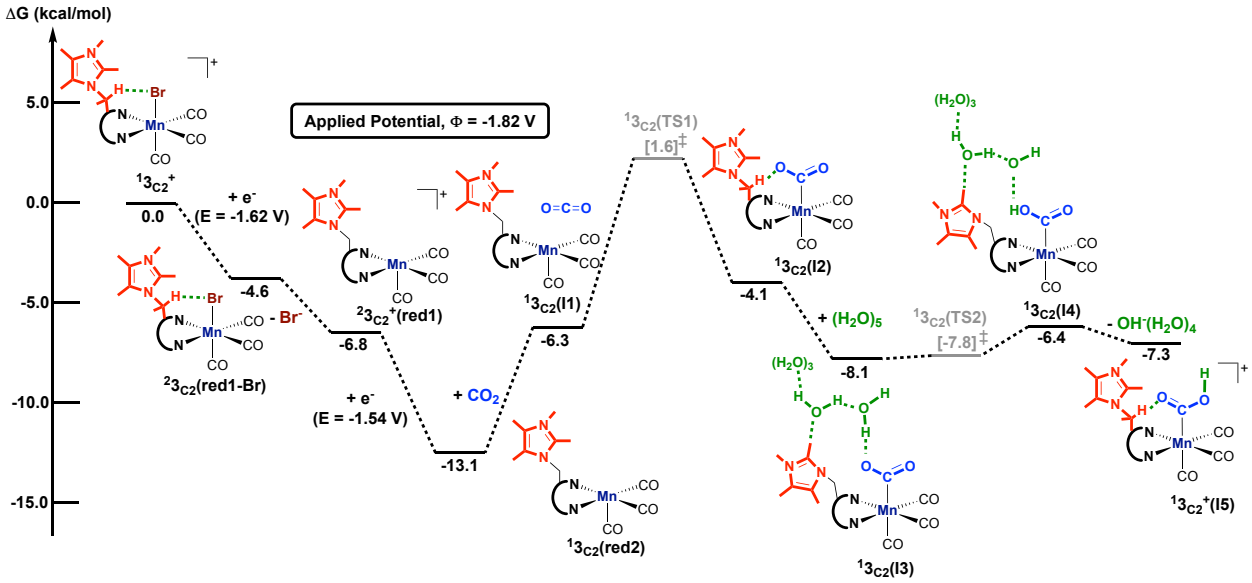


**Figure S5**. Computed free energy (kcal/mol) profile for the formation of the metallocarboxylic acid species, $\mathbf{3_{C2}^{+}(I5)}$. All free energies are calculated with respect to the separated reactants and the superscript corresponds to the spin multiplicity of a given species. The computed electronic energy for $\mathbf{3_{C2}(TS2)}$ is higher than that of $\mathbf{3_{C2}(I4)}$. However, $\mathbf{3_{C2}(TS2)}$ has a lower zero-point energy, offsetting its higher Gibbs free energy.

In $H_2O$, the formation of the metallocarboxylic acid species $\mathbf{2_{C5}^{+}(I5)}$ and $\mathbf{3_{C2}^{+}(I5)}$ is downhill by 4.9 kcal/mol and 3.2 kcal/mol, respectively, with respect to the metallocarboxylate complexes (Figures S4 and S5). In this case, the computed transition states for forming the metalocarboxylic acid species, $\mathbf{2_{C5}(TS2)}$ and $\mathbf{3_{C2}(TS2)}$, have computed free energies of -8.4 kcal/mol and -7.8 kcal/mol, respectively, which are higher in energy than for $\mathbf{1_{C2}(TS2)}$ ($\Delta$G = -8.8 kcal/mol, Figure 3). Interestingly, the optimized geometries suggest that the C5-H or C2-$CH_3$ groups on the imidazolium ligand interact with the water cluster and assist the proton transfer from $H_2O$ to the carboxyl group. The strength of such facilitation directly depends on the substituents at the C2

and C4/C5 positions of the imidazolium moiety. For instance, $\mathbf{2_{C5}(TS2)}$ features a hydrogen-bonding interaction of C5-H···$OH_2$ = 2.07 Å between the imidazolium ligand and the water cluster, and an additional interaction of 2.19 Å between $H_2O$ and the bridging methylene ligand (Figure S8).

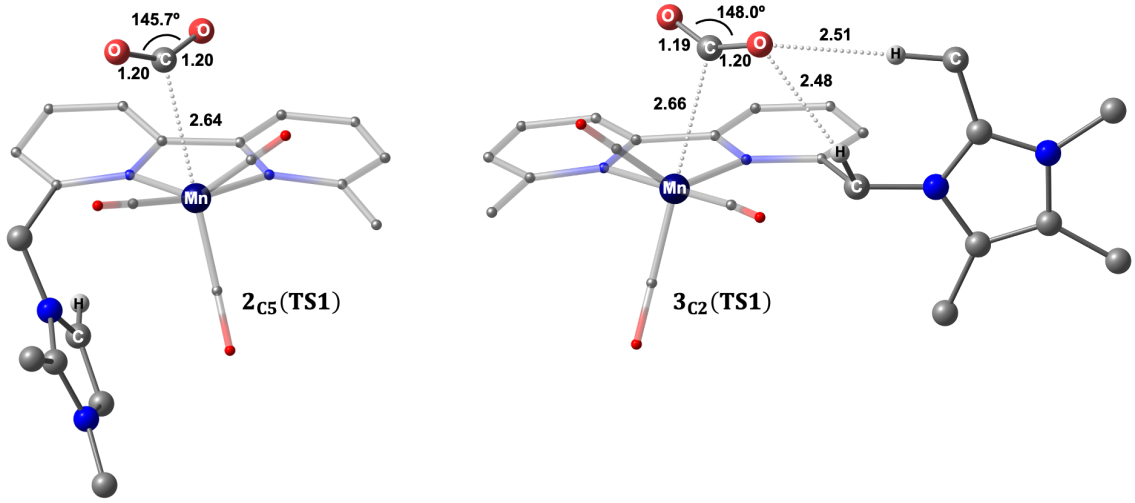


**Figure S6.** Optimized geometries of the transition state $\mathbf{2_{C5}(TS1)}$ (left) and $\mathbf{3_{C2}(TS1)}$ (right) for the formation of the Mn-$CO_2$ adduct. Distances are given in angstroms, and bond angles are in degrees. Non-participating hydrogen atoms are omitted for clarity.

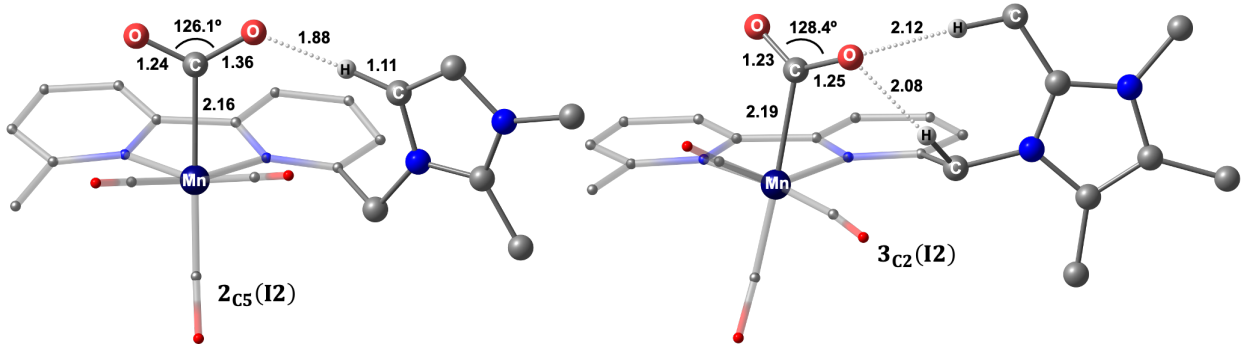


**Figure S7.** Optimized geometries of the metallocarboxylate in $\mathbf{2_{C5}(I2)}$ (left) and $\mathbf{3_{C2}(I2)}$ (right). Distances are given in angstroms, and bond angles are in degrees. Non-participating hydrogen atoms are omitted for clarity.

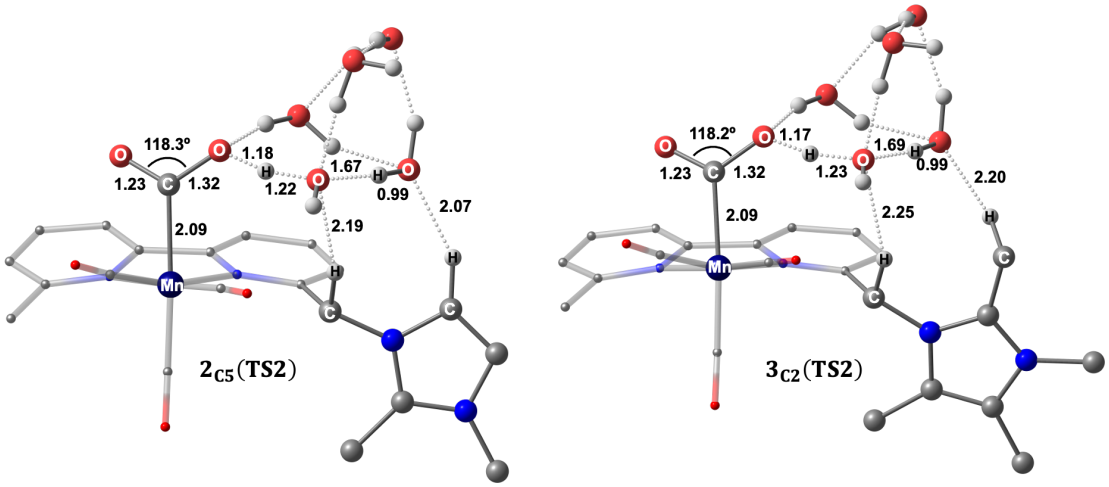


**Figure S8.** Optimized geometries of the transition state $\mathbf{2_{C5}(TS2)}$ (left) and $\mathbf{3_{C2}(TS2)}$ (right) for the formation of the metallocarboxylic acid species. Distances are given in angstroms, and bond angles are in degrees. Non-participating hydrogen atoms are omitted for clarity.

**2.2. Reduction-first pathway versus protonation-first pathway from $\mathbf{2}^{+}_{\mathbf{C5}}(\mathbf{I5})$ and $\mathbf{3}^{+}_{\mathbf{C2}}(\mathbf{I5})$.** Following the formation of the metallocarboxylic acid species $\mathbf{2}^{+}_{\mathbf{C5}}(\mathbf{I5})$ and $\mathbf{3}^{+}_{\mathbf{C2}}(\mathbf{I5})$, the Gibbs free energy reaction profiles for the reduction-first and protonation-first pathways were considered for the second and third catalysts (Figures S9 and S10).

For the reduction-first mechanism, the calculated reductions potentials for $\mathbf{2}^{+}_{\mathbf{C5}}(\mathbf{I5})$ to $\mathbf{2}_{\mathbf{C5}}(\mathbf{I5\text{-}R})$ and $\mathbf{3}^{+}_{\mathbf{C2}}(\mathbf{I5})$ to $\mathbf{3}_{\mathbf{C2}}(\mathbf{I5\text{-}R})$ are, respectively, -1.67 V and -1.66 V versus the $Fc^{0/+}$ couple. These redox potentials are, as seen for **1**$^{+}$, in the potential range where the catalytic current of **2**$^{+}$ and **3**$^{+}$ were observed experimentally.[3] Presumably, the reduction-first pathway is preferred experimentally under an applied potential of Φ = -1.82 V for all catalysts. As seen in $\mathbf{1}^{+}_{\mathbf{C2}}$, both the imidazolium moiety and bridging methylene ligand interact with the proton source to assist the C-O bond cleavage step and generate the neutral tetracarbonyl species (Figure S11). It can also be noted that stronger hydrogen-bonding interactions are formed between the imidazolium moiety and water in compound **1**$^{+}$ (C2-H$\cdots$$OH_2$ = 1.89 Å, Figure 8) than in the second and third catalysts (C5-H$\cdots$$OH_2$ = 2.00 Å in **2**$^{+}$ and C2-$CH_3\cdots OH_2$ = 2.17 Å in **3**$^{+}$, Figure S11). These weaker interactions in going from **1**$^{+}$ to **3**$^{+}$ are compensated by slightly stronger hydrogen-bonding interactions between the methylene bridging ligand and $H_2O$ (H$\cdots$$OH_2$ = 2.43 Å in **1**$^{+}$; H$\cdots$$OH_2$ = 2.39 Å in **2**$^{+}$; H$\cdots$$OH_2$ = 2.34 Å in **3**$^{+}$, Figures 8 and S11).

Overall, the calculated Gibbs free energy reaction profiles for the protonation-first and reduction-first pathways are competitive, meaning that both of the reduction-first and protonation-first pathways are accessible experimentally. However, as previously stated, we hypothesize that the higher catalytic activity, which occurs between -1.50 V to -1.80 V, is due to the reduction-first pathway.[3] Finally, after the removal of hydroxyl, the neutral tetracarbonyl intermediates $\mathbf{2}^{+}_{\mathbf{C5}}(\mathbf{I8})$ and $\mathbf{3}^{+}_{\mathbf{C2}}(\mathbf{I8})$ are produced, and can be reduced at -1.51 V and -1.53 V to yield, respectively, $\mathbf{2}_{\mathbf{C5}}(\mathbf{red2})$ and $\mathbf{3}_{\mathbf{C2}}(\mathbf{red2})$ along with CO dissociation (Figures S9 and S10).

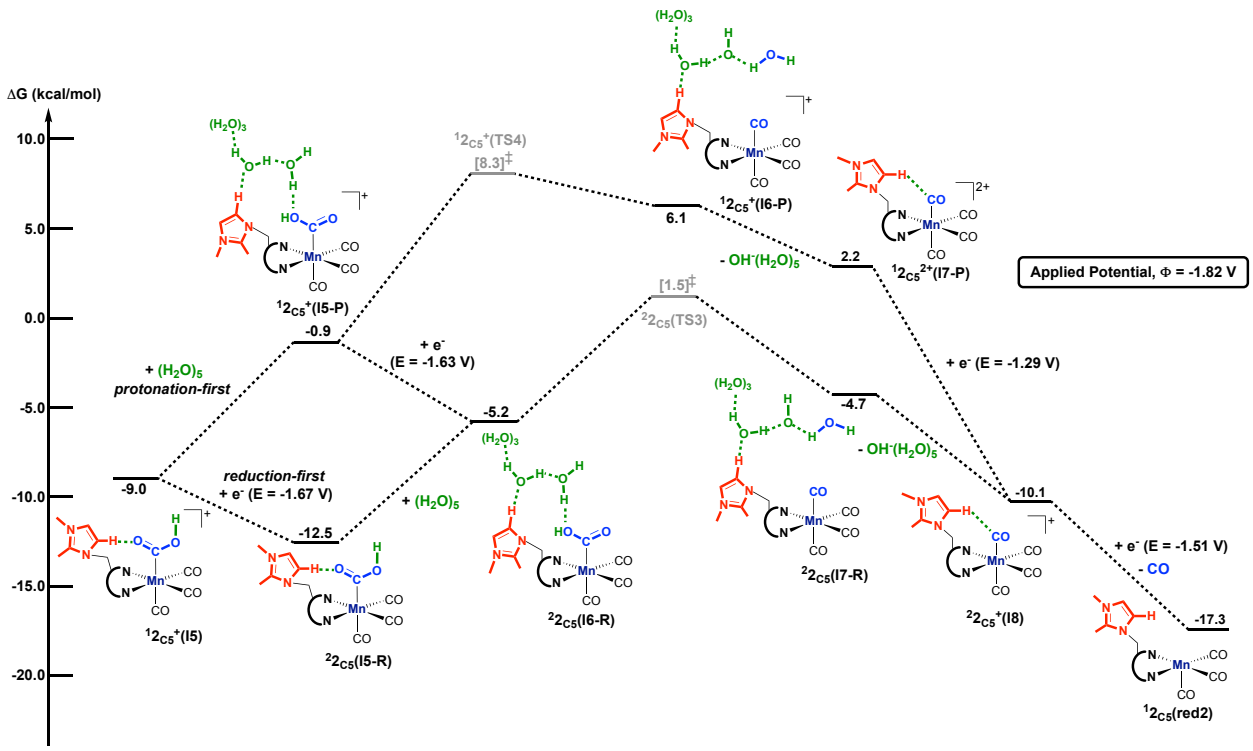


**Figure S9.** Computed free energy (kcal/mol) profile for the protonation-first and reduction-first pathway from intermediate $\mathbf{2^{+}_{C5}(I5)}$ in the presence of water. All free energies are calculated with respect to the separated reactants and the superscript represents the spin multiplicity of a given species.

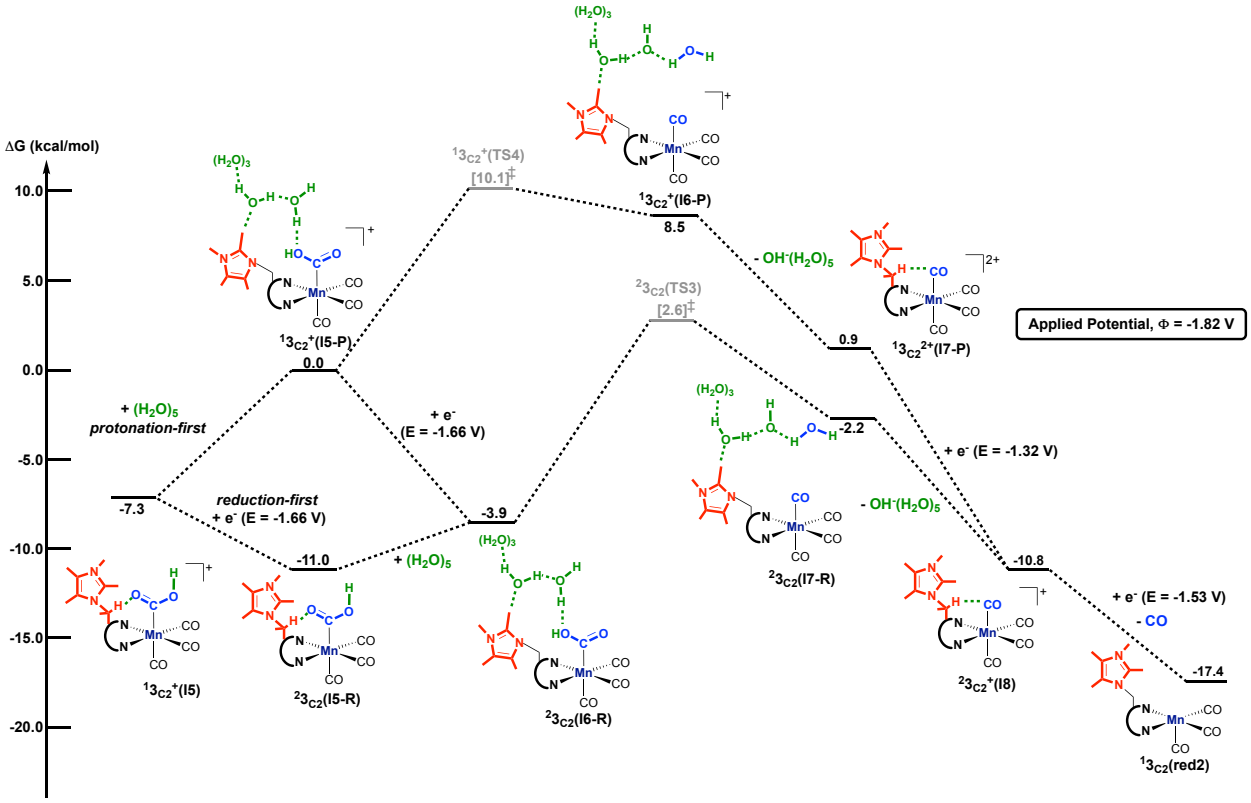


**Figure S10.** Computed free energy (kcal/mol) profile for the protonation-first and reduction-first pathway from intermediate $\mathbf{3^{+}_{C2}(I5)}$ in the presence of water. All free energies are calculated with respect to the separated reactants and the superscript represents the spin multiplicity of a given species.

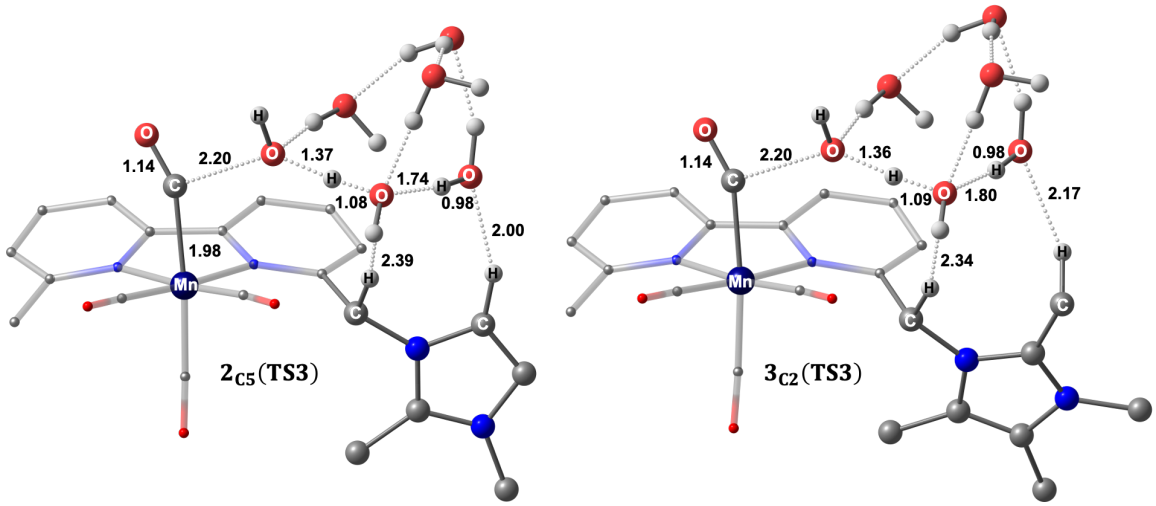


**Figure S11.** Optimized geometries of the transition state $\mathbf{2_{C5}(TS3)}$ (left) and $\mathbf{3_{C2}(TS3)}$ (right) for the C-O bond cleavage step. Distances are given in angstroms, and non-participating hydrogen atoms are omitted for clarity.

## 2.3. Computed reaction profiles for $CO_2$-to-CO conversion using $\mathbf{1}_{C5}^{+}$, $\mathbf{2}_{C2}^{+}$ and $\mathbf{3}_{C5}^{+}$.

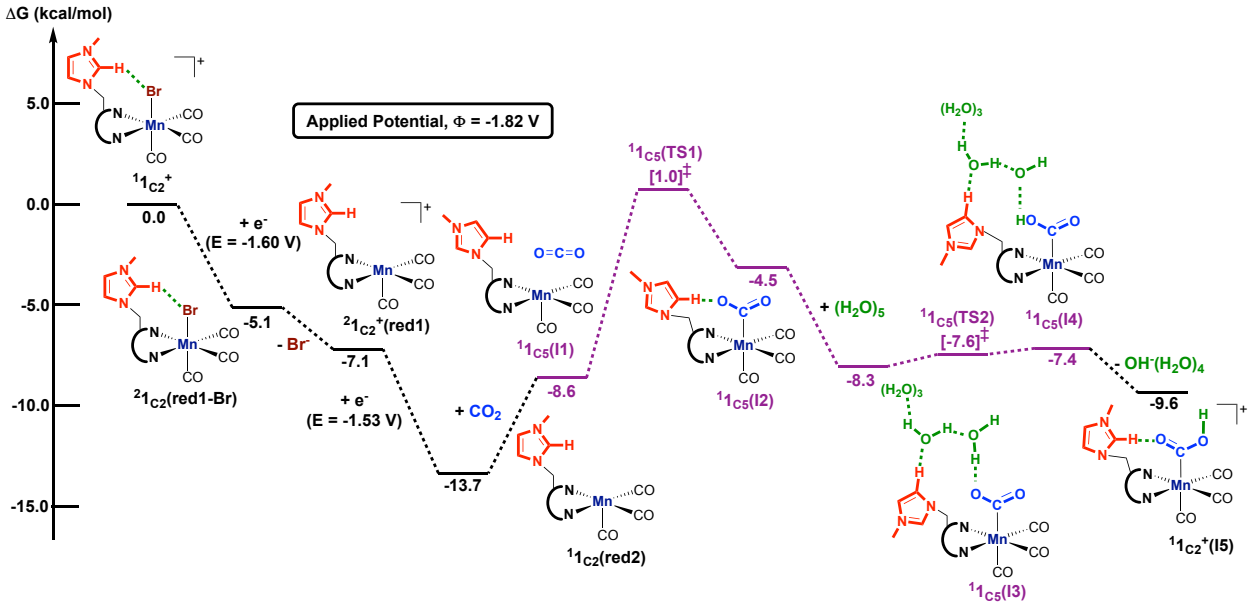


**Figure S12**. Computed free energy (kcal/mol) profile for the formation of the metallocarboxylic acid species, $\mathbf{1}_{C2}^{+}(\mathbf{I5})$. The transition states and intermediates that involve the C4/C5-H substituent on the imidazolium moiety are highlighted in purple. To compare the effect of the C2-H and C4/C5-H substituents during catalysis, all free energies are calculated with respect to a common reference ($\mathbf{1}_{C2}^{+}$, $CO_2$ and $(H_2O)_5$ in a chair configuration). We note that $\mathbf{1}_{C2}^{+}(\mathbf{I5})$ is lower in energy than $\mathbf{1}_{C5}^{+}(\mathbf{I5})$ by 1.2 kcal/mol. Therefore, this intermediate was used as a reference for the reduction-first versus protonation-first pathways (Figure S13). The superscript corresponds to the spin multiplicity of a given species.

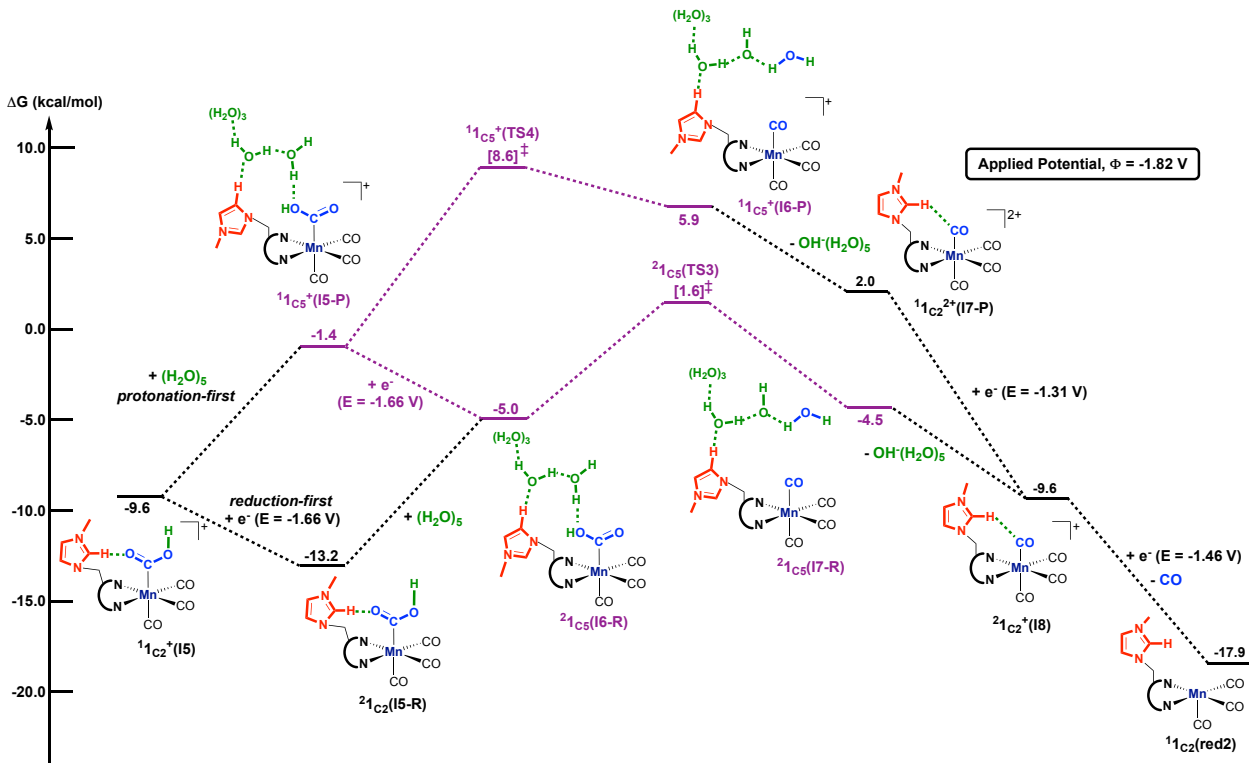


**Figure S13.** Computed free energy (kcal/mol) profile for the protonation-first and reduction-first pathway from intermediate $\mathbf{1}_{\mathbf{C2}}^{+}(\mathbf{I5})$ in the presence of a $(H_2O)_5$ cluster. The transition states and intermediates that involve the C4/C5-H substituent on the imidazolium moiety are highlighted in purple. To compare the effect of the C2-H and C4/C5-H substituents during catalysis, all free energies are calculated with respect to a common reference ($\mathbf{1}_{\mathbf{C2}}^{+}(\mathbf{I5})$, $CO_2$ and $(H_2O)_5$ in a chair configuration).

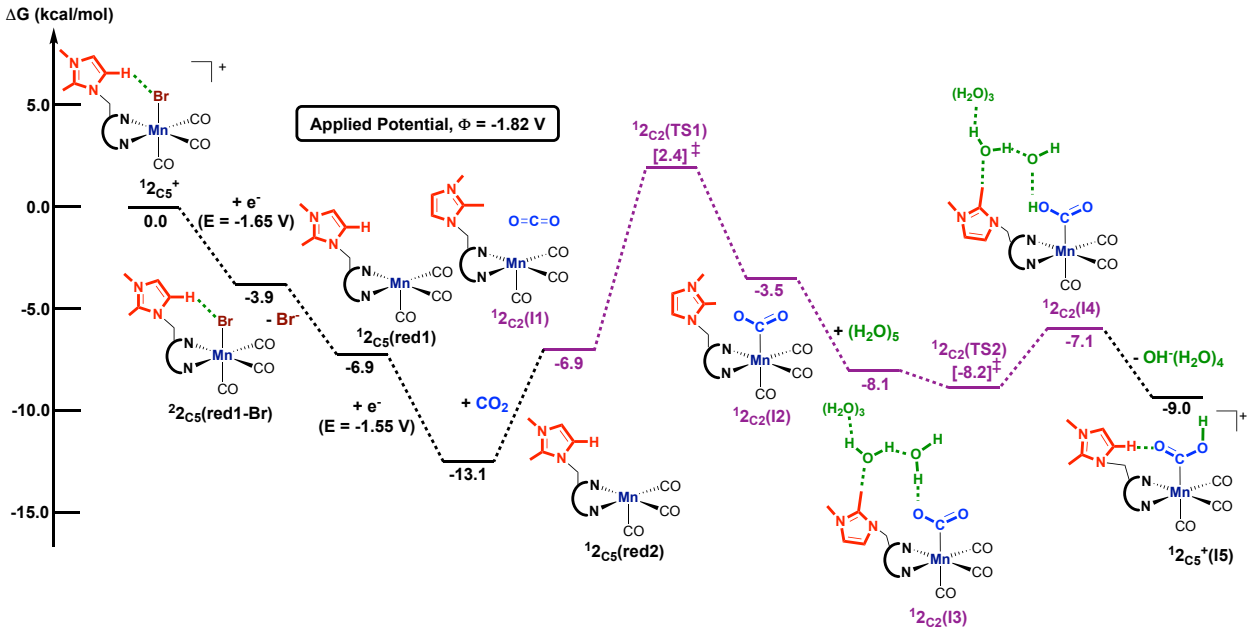


**Figure S14**. Computed free energy (kcal/mol) profile for the formation of the metallocarboxylic acid species, $\mathbf{2^+_{C2}(I5)}$. The transition states and intermediates that involve the C2-$CH_3$ substituent on the imidazolium moiety are highlighted in purple. To compare the effect of the C2-$CH_3$ and C4/C5-H substituents during catalysis, all free energies are calculated with respect to a common reference ($\mathbf{2^+_{C5}}$, $CO_2$ and $(H_2O)_5$ in a chair configuration). We note that $\mathbf{2^+_{C5}(I5)}$ is lower in energy than $\mathbf{2^+_{C2}(I5)}$ by 1.3 kcal/mol. Therefore, this intermediate was used as a reference for the reduction-first versus protonation-first pathways (Figure S15). The superscript corresponds to the spin multiplicity of a given species.

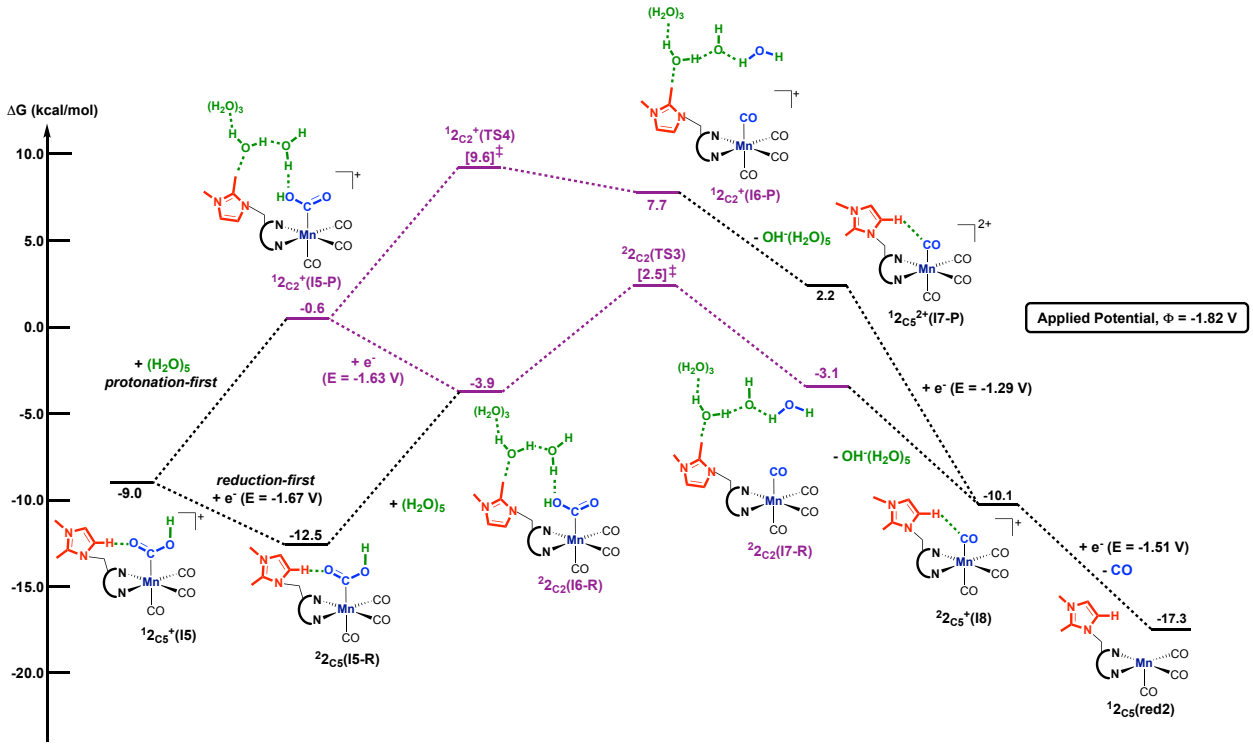


**Figure S15.** Computed free energy (kcal/mol) profile for the protonation-first and reduction-first pathway from intermediate $\mathbf{2^{+}_{C5}(I5)}$ in the presence of a $(H_2O)_5$ cluster. The transition states and intermediates that involve the C2-$CH_3$ substituent on the imidazolium moiety are highlighted in purple. To compare the effect of the C2-$CH_3$ and C4/C5-H substituents during catalysis, all free energies are calculated with respect to a common reference ($\mathbf{2^{+}_{C5}(I5)}$, $CO_2$ and $(H_2O)_5$ in a chair configuration). The superscript corresponds to the spin multiplicity of a given species.

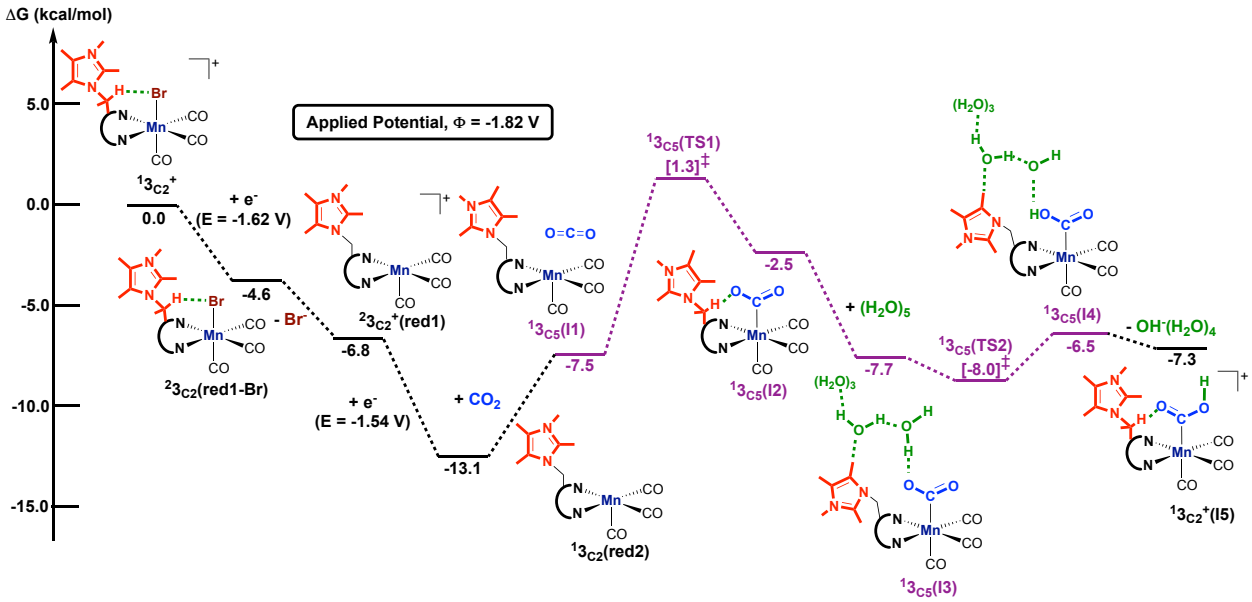


**Figure S16**. Computed free energy (kcal/mol) profile for the formation of the metallocarboxylic acid species, $\mathbf{3_{C2}^{+}(I5)}$. The transition states and intermediates that involve the C4/C5-$CH_3$ substituent on the imidazolium moiety are highlighted in purple. To compare the effect of the C2-$CH_3$ and C4/C5-$CH_3$ substituents during catalysis, all free energies are calculated with respect to a common reference ($\mathbf{3_{C2}^{+}}$, $CO_2$ and $(H_2O)_5$ in a chair configuration). We note that $\mathbf{3_{C2}^{+}(I5)}$ is lower in energy than $\mathbf{3_{C5}^{+}(I5)}$ by 1.0 kcal/mol. Therefore, this intermediate was used as a reference for the reduction-first versus protonation-first pathways (Figure S17). The superscript corresponds to the spin multiplicity of a given species.

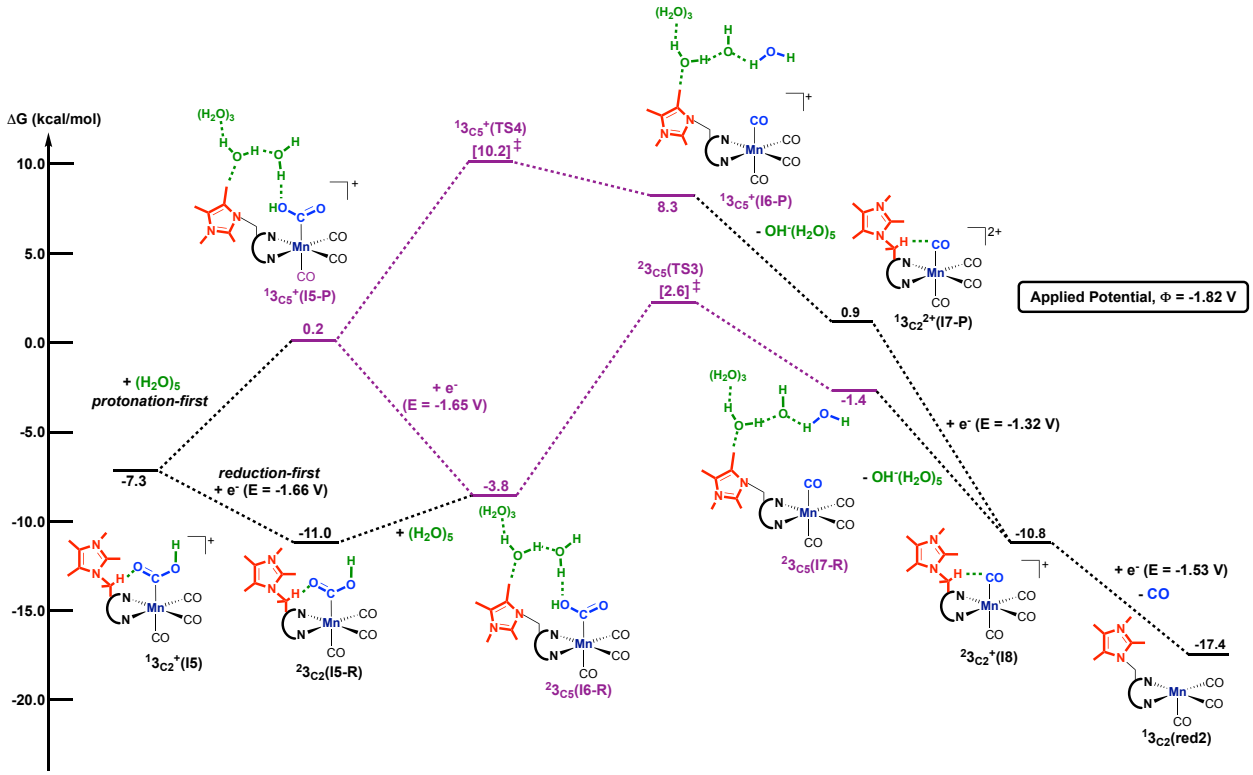


**Figure S17.** Computed free energy (kcal/mol) profile for the protonation-first and reduction-first pathway from intermediate $\mathbf{3^{+}_{C2}(I5)}$ in the presence of a $(H_2O)_5$ cluster. The transition states and intermediates that involve the C4/C5-$CH_3$ substituent on the imidazolium moiety are highlighted in purple. To compare the effect of the C2-$CH_3$ and C4/C5-$CH_3$ substituents during catalysis, all free energies are calculated with respect to a common reference ($\mathbf{3^{+}_{C2}(I5)}$, $CO_2$ and $(H_2O)_5$ in a chair configuration). The superscript corresponds to the spin multiplicity of a given species.

**2.4. Calculated redox potentials, turnover frequencies and "degrees of TOF control" for all species.**

**Table S1.** Calculated reduction potentials (in V versus the $Fc^{0/+}$ couple) at the ωB97X-D(SMD)/BS2//ωB97X-D(SMD)BS1 level of theory for the one- and two-electron reduced species of all three catalysts. $E_1^{1/2}$ (calc.) is the calculated redox potential for the first reduction of the six-to-six coordinate species while $E_2^{1/2}$ (calc.) is the second reduction potential for the five-to-five coordinate species (after initial bromide dissociation). Experimentally, complexes **$1^+$-$3^+$** exhibit two coalesced 1e- reductions ranging from -1.49 V to -1.53 V versus the $Fc^{0/+}$ couple, which is in good agreement with our calculated redox potentials.[3]

| **Catalysts** | $E_1^{1/2}$ (calc.) | $E_2^{1/2}$ (calc.) |
|---|---|---|
| $\mathbf{1}^+_{\mathbf{C2}}$ | -1.60 | **-1.53** |
| $\mathbf{1}^+_{\mathbf{C5}}$ | -1.64 | **-1.53** |
| $\mathbf{2}^+_{\mathbf{C5}}$ | -1.65 | **-1.55** |
| $\mathbf{2}^+_{\mathbf{C2}}$ | -1.60 | **-1.55** |
| $\mathbf{3}^+_{\mathbf{C2}}$ | -1.62 | **-1.54** |
| $\mathbf{3}^+_{\mathbf{C5}}$ | -1.69 | **-1.57** |

**Table S2.** Steps considered to calculate the TOF and $X_{TOF}$ using $\mathbf{1}_{\mathbf{C2}}^{+}$ for the $CO_2$ reduction reaction ($CO_2$RR) under an applied potential of Φ = −1.82 V versus the $Fc^{0/+}$ couple. The TOF is calculated to be 5.8E01 $s^{-1}$ at the ωB97X-D(SMD)/BS2//ωB97X-D(SMD)BS1 level of theory. The "degree of TOF control" ($X_{TOF}$) for the intermediates and transition states are given in Table S3. [a]The Gibbs free energy of the highest intermediate was employed for the transition state. The overall change in the Gibbs free energy is -4.2 kcal/mol. The TOF determining intermediate (TDI) and the TOF determining transition state (TDTS) based on the energy span model are highlighted in gray.

| | **Intermediates, $I_j$ (kcal/mol)** | | **Transition States, $T_i$ (kcal/mol)** | |
|---|---|---|---|---|
| **Step 1** | 0.0 | $\mathbf{1}_{\mathbf{C2}}^{+}$ | 0.0 | |
| **Step 2** | -5.1 | $\mathbf{1}_{\mathbf{C2}}(\mathbf{red1\text{-}Br})$ | -5.1 | |
| **Step 3** | -7.1 | $\mathbf{1}_{\mathbf{C2}}^{+}(\mathbf{red1})$ | -7.1 | |
| **Step 4** | -13.7 | $\mathbf{1}_{\mathbf{C2}}(\mathbf{red2})$ | -8.4 | |
| **Step 5** | -8.4 | $\mathbf{1}_{\mathbf{C2}}(\mathbf{I1})$ | 0.7 | $\mathbf{1}_{\mathbf{C2}}(\mathbf{TS1})$ |
| **Step 6** | -6.7 | $\mathbf{1}_{\mathbf{C2}}(\mathbf{I2})$ | -6.7 | |
| **Step 7** | -8.2 | $\mathbf{1}_{\mathbf{C2}}(\mathbf{I3})$ | -7.9[a] | $\mathbf{1}_{\mathbf{C2}}(\mathbf{TS2})$ |
| **Step 8** | -7.9 | $\mathbf{1}_{\mathbf{C2}}(\mathbf{I4})$ | -7.9 | |
| **Step 9** | -9.6 | $\mathbf{1}_{\mathbf{C2}}^{+}(\mathbf{I5})$ | -9.6 | |
| **Step 10** | 13.2 | $\mathbf{1}_{\mathbf{C2}}(\mathbf{I5\text{-}R})$ | -5.8 | |
| **Step 11** | -5.8 | $\mathbf{1}_{\mathbf{C2}}(\mathbf{I6\text{-}R})$ | 0.9 | $\mathbf{1}_{\mathbf{C2}}(\mathbf{TS3})$ |
| **Step 12** | -5.4 | $\mathbf{1}_{\mathbf{C2}}(\mathbf{I7\text{-}R})$ | -5.4 | |
| **Step 13** | -9.6 | $\mathbf{1}_{\mathbf{C2}}^{+}(\mathbf{I8})$ | -9.6 | |

**Table S3.** $X_{TOF}$ of each intermediate and transition state using $\mathbf{1}_{C2}^{+}$ for $CO_2RR$ under an applied potential of Φ = −1.82 V versus the $Fc^{0/+}$ couple. The "degree of TOF control" for the TOF determining intermediate (TDI) and the TOF determining transition state (TDTS) based on the energy span model are highlighted in gray.

| | $X_{TOF}$, $I_j$ | | $X_{TOF}$, $T_i$ | |
|---|---|---|---|---|
| **Step 1** | 0.00 | $\mathbf{1}_{C2}^{+}$ | 0.00 | |
| **Step 2** | 0.00 | $\mathbf{1}_{C2}(\mathbf{red1\text{-}Br})$ | 0.00 | |
| **Step 3** | 0.00 | $\mathbf{1}_{C2}^{+}(\mathbf{red1})$ | 0.00 | |
| **Step 4** | 0.80 | $\mathbf{1}_{C2}(\mathbf{red2})$ | 0.00 | |
| **Step 5** | 0.00 | $\mathbf{1}_{C2}(\mathbf{I1})$ | 0.33 | $\mathbf{1}_{C2}(\mathbf{TS1})$ |
| **Step 6** | 0.00 | $\mathbf{1}_{C2}(\mathbf{I2})$ | 0.00 | |
| **Step 7** | 0.00 | $\mathbf{1}_{C2}(\mathbf{I3})$ | 0.00 | $\mathbf{1}_{C2}(\mathbf{TS2})$ |
| **Step 8** | 0.00 | $\mathbf{1}_{C2}(\mathbf{I4})$ | 0.00 | |
| **Step 9** | 0.00 | $\mathbf{1}_{C2}^{+}(\mathbf{I5})$ | 0.00 | |
| **Step 10** | 0.20 | $\mathbf{1}_{C2}(\mathbf{I5\text{-}R})$ | 0.00 | |
| **Step 11** | 0.00 | $\mathbf{1}_{C2}(\mathbf{I6\text{-}R})$ | 0.67 | $\mathbf{1}_{C2}(\mathbf{TS3})$ |
| **Step 12** | 0.00 | $\mathbf{1}_{C2}(\mathbf{I7\text{-}R})$ | 0.00 | |
| **Step 13** | 0.00 | $\mathbf{1}_{C2}^{+}(\mathbf{I8})$ | 0.00 | |

**Table S4.** Steps considered to calculate the TOF and $X_{TOF}$ using $\mathbf{1}_{\mathbf{C2}}^{+}$ for the hydrogen evolution reaction (HER) under an applied potential of Φ = −1.82 V versus the $Fc^{0/+}$ couple. The TOF is calculated to be 1.6E-03 $s^{-1}$ at the ωB97X-D(SMD)/BS2//ωB97X-D(SMD)BS1 level of theory. The "degree of TOF control" ($X_{TOF}$) for the intermediates and transition states are given in Table S5. The overall change in the Gibbs free energy is -19.1 kcal/mol. The TOF determining intermediate (TDI) and the TOF determining transition state (TDTS) based on the energy span model are highlighted in gray.

| | **Intermediates, $I_j$ (kcal/mol)** | | **Transition States, $T_i$ (kcal/mol)** | |
|---|---|---|---|---|
| **Step 1** | 0.0 | $\mathbf{1}_{\mathbf{C2}}^{+}$ | 0.0 | |
| **Step 2** | -5.1 | $\mathbf{1}_{\mathbf{C2}}(\mathbf{red1\text{-}Br})$ | -5.1 | |
| **Step 3** | -7.1 | $\mathbf{1}_{\mathbf{C2}}^{+}(\mathbf{red1})$ | -7.1 | |
| **Step 4** | -13.7 | $\mathbf{1}_{\mathbf{C2}}(\mathbf{red2})$ | -8.3 | |
| **Step 5** | -8.3 | $\mathbf{1}_{\mathbf{C2}}(\mathbf{I9})$ | 7.0 | $\mathbf{1}_{\mathbf{C2}}(\mathbf{TS5})$ |
| **Step 6** | -12.1 | $\mathbf{1}_{\mathbf{C2}}(\mathbf{I10})$ | -12.1 | |
| **Step 7** | -20.2 | $\mathbf{1}_{\mathbf{C2}}^{+}(\mathbf{I11})$ | -20.2 | |
| **Step 8** | -23.2 | $\mathbf{1}_{\mathbf{C2}}(\mathbf{I11\text{-}R})$ | -15.5 | |
| **Step 9** | -15.5 | $\mathbf{1}_{\mathbf{C2}}(\mathbf{I12\text{-}R})$ | -2.2 | $\mathbf{1}_{\mathbf{C2}}(\mathbf{TS6})$ |
| **Step 10** | -5.6 | $\mathbf{1}_{\mathbf{C2}}(\mathbf{I13\text{-}R})$ | -5.6 | |
| **Step 11** | -10.3 | $\mathbf{1}_{\mathbf{C2}}^{+}(\mathbf{I14})$ | -10.3 | |
| **Step 12** | -26.2 | $\mathbf{1}_{\mathbf{C2}}^{+}(\mathbf{red1})$ | -26.2 | |

**Table S5.** $X_{TOF}$ of each intermediate and transition state using $\mathbf{1}_{C2}^{+}$ for HER under an applied potential of Φ = −1.82 V versus the $Fc^{0/+}$ couple. The "degree of TOF control" for the TOF determining intermediate (TDI) and the TOF determining transition state (TDTS) based on the energy span model are highlighted in gray.

| | $X_{TOF}$, $I_j$ | | $X_{TOF}$, $T_i$ | |
|---|---|---|---|---|
| **Step 1** | 0.00 | $\mathbf{1}_{C2}^{+}$ | 0.00 | |
| **Step 2** | 0.00 | $\mathbf{1}_{C2}$(**red1-Br**) | 0.00 | |
| **Step 3** | 0.00 | $\mathbf{1}_{C2}^{+}$(**red1**) | 0.00 | |
| **Step 4** | 0.37 | $\mathbf{1}_{C2}$(**red2**) | 0.00 | |
| **Step 5** | 0.00 | $\mathbf{1}_{C2}$(**I9**) | 0.37 | $\mathbf{1}_{C2}$(**TS5**) |
| **Step 6** | 0.00 | $\mathbf{1}_{C2}$(**I10**) | 0.00 | |
| **Step 7** | 0.01 | $\mathbf{1}_{C2}^{+}$(**I11**) | 0.00 | |
| **Step 8** | 0.62 | $\mathbf{1}_{C2}$(**I11-R**) | 0.00 | |
| **Step 9** | 0.00 | $\mathbf{1}_{C2}$(**I12-R**) | 0.62 | $\mathbf{1}_{C2}$(**TS6**) |
| **Step 10** | 0.00 | $\mathbf{1}_{C2}$(**I13-R**) | 0.00 | |
| **Step 11** | 0.00 | $\mathbf{1}_{C2}^{+}$(**I14**) | 0.00 | |
| **Step 12** | 0.00 | $\mathbf{1}_{C2}^{+}$(**red1**) | 0.00 | |

**Table S6.** Steps considered to calculate the TOF and $X_{TOF}$ using $\mathbf{1}_{\mathbf{C5}}^{+}$ for $CO_2RR$ under an applied potential of Φ = −1.82 V versus the $Fc^{0/+}$ couple. The TOF is calculated to be 2.2E+01 $s^{-1}$ at the ωB97X-D(SMD)/BS2//ωB97X-D(SMD)BS1 level of theory. The "degree of TOF control" ($X_{TOF}$) for the intermediates and transition states are given in Table S7. [a]The Gibbs free energy of the highest intermediate was employed for the transition state. The overall change in the Gibbs free energy is -4.2 kcal/mol. The TOF determining intermediate (TDI) and the TOF determining transition state (TDTS) based on the energy span model are highlighted in gray.

| | **Intermediates, $I_j$ (kcal/mol)** | | **Transition States, $T_i$ (kcal/mol)** | |
|---|---|---|---|---|
| **Step 1** | 0.0 | $\mathbf{1}_{\mathbf{C2}}^{+}$ | 0.0 | |
| **Step 2** | -5.1 | $\mathbf{1}_{\mathbf{C2}}(\mathbf{red1\text{-}Br})$ | -5.1 | |
| **Step 3** | -7.1 | $\mathbf{1}_{\mathbf{C2}}^{+}(\mathbf{red1})$ | -7.1 | |
| **Step 4** | -13.7 | $\mathbf{1}_{\mathbf{C2}}(\mathbf{red2})$ | -8.6 | |
| **Step 5** | -8.6 | $\mathbf{1}_{\mathbf{C5}}(\mathbf{I1})$ | 0.9 | $\mathbf{1}_{\mathbf{C5}}(\mathbf{TS1})$ |
| **Step 6** | -4.5 | $\mathbf{1}_{\mathbf{C5}}(\mathbf{I2})$ | -4.5 | |
| **Step 7** | -8.3 | $\mathbf{1}_{\mathbf{C5}}(\mathbf{I3})$ | -7.4[a] | $\mathbf{1}_{\mathbf{C5}}(\mathbf{TS2})$ |
| **Step 8** | -7.4 | $\mathbf{1}_{\mathbf{C5}}(\mathbf{I4})$ | -7.4 | |
| **Step 9** | -9.6 | $\mathbf{1}_{\mathbf{C2}}^{+}(\mathbf{I5})$ | -9.6 | |
| **Step 10** | -13.2 | $\mathbf{1}_{\mathbf{C2}}(\mathbf{I5\text{-}R})$ | -5.0 | |
| **Step 11** | -5.0 | $\mathbf{1}_{\mathbf{C5}}(\mathbf{I6\text{-}R})$ | 1.6 | $\mathbf{1}_{\mathbf{C5}}(\mathbf{TS3})$ |
| **Step 12** | -4.5 | $\mathbf{1}_{\mathbf{C5}}(\mathbf{I7\text{-}R})$ | -4.5 | |
| **Step 13** | -9.6 | $\mathbf{1}_{\mathbf{C2}}^{+}(\mathbf{I8})$ | -9.6 | |

**Table S7.** $X_{TOF}$ of each intermediate and transition state using $\mathbf{1}_{C5}^{+}$ for $CO_2RR$ under an applied potential of Φ = −1.82 V versus the $Fc^{0/+}$ couple. The "degree of TOF control" for the TOF determining intermediate (TDI) and the TOF determining transition state (TDTS) based on the energy span model are highlighted in gray.

| | $X_{TOF}$, $I_j$ | | $X_{TOF}$, $T_i$ | |
|---|---|---|---|---|
| **Step 1** | 0.00 | $\mathbf{1}_{C2}^{+}$ | 0.00 | |
| **Step 2** | 0.00 | $\mathbf{1}_{C2}(\mathbf{red1\text{-}Br})$ | 0.00 | |
| **Step 3** | 0.00 | $\mathbf{1}_{C2}^{+}(\mathbf{red1})$ | 0.00 | |
| **Step 4** | 0.75 | $\mathbf{1}_{C2}(\mathbf{red2})$ | 0.00 | |
| **Step 5** | 0.00 | $\mathbf{1}_{C5}(\mathbf{I1})$ | 0.18 | $\mathbf{1}_{C5}(\mathbf{TS1})$ |
| **Step 6** | 0.00 | $\mathbf{1}_{C5}(\mathbf{I2})$ | 0.00 | |
| **Step 7** | 0.00 | $\mathbf{1}_{C5}(\mathbf{I3})$ | 0.00 | $\mathbf{1}_{C5}(\mathbf{TS2})$ |
| **Step 8** | 0.00 | $\mathbf{1}_{C5}(\mathbf{I4})$ | 0.00 | |
| **Step 9** | 0.00 | $\mathbf{1}_{C2}^{+}(\mathbf{I5})$ | 0.00 | |
| **Step 10** | 0.25 | $\mathbf{1}_{C2}(\mathbf{I5\text{-}R})$ | 0.00 | |
| **Step 11** | 0.00 | $\mathbf{1}_{C5}(\mathbf{I6\text{-}R})$ | 0.82 | $\mathbf{1}_{C5}(\mathbf{TS3})$ |
| **Step 12** | 0.00 | $\mathbf{1}_{C5}(\mathbf{I7\text{-}R})$ | 0.00 | |
| **Step 13** | 0.00 | $\mathbf{1}_{C2}^{+}(\mathbf{I8})$ | 0.00 | |

**Table S8.** Steps considered to calculate the TOF and $X_{TOF}$ using $\mathbf{2}_{\mathbf{C5}}^{+}$ for $CO_2RR$ under an applied potential of Φ = −1.82 V versus the $Fc^{0/+}$ couple. The TOF is calculated to be 2.4E+01 $s^{-1}$ at the ωB97X-D(SMD)/BS2//ωB97X-D(SMD)BS1 level of theory. The "degree of TOF control" ($X_{TOF}$) for the intermediates and transition states are given in Table S9. [a]The Gibbs free energy of the highest intermediate was employed for the transition state. The overall change in the Gibbs free energy is -4.2 kcal/mol. The TOF determining intermediate (TDI) and the TOF determining transition state (TDTS) based on the energy span model are highlighted in gray.

| | **Intermediates, $I_j$ (kcal/mol)** | | **Transition States, $T_i$ (kcal/mol)** | |
|---|---|---|---|---|
| **Step 1** | 0.0 | $\mathbf{2}_{\mathbf{C5}}^{+}$ | 0.0 | |
| **Step 2** | -3.9 | $\mathbf{2}_{\mathbf{C5}}(\mathbf{red1\text{-}Br})$ | -3.9 | |
| **Step 3** | -6.9 | $\mathbf{2}_{\mathbf{C5}}^{+}(\mathbf{red1})$ | -6.9 | |
| **Step 4** | -13.1 | $\mathbf{2}_{\mathbf{C5}}(\mathbf{red2})$ | -7.5 | |
| **Step 5** | -7.5 | $\mathbf{2}_{\mathbf{C5}}(\mathbf{I1})$ | 2.3 | $\mathbf{2}_{\mathbf{C5}}(\mathbf{TS1})$ |
| **Step 6** | -4.1 | $\mathbf{2}_{\mathbf{C5}}(\mathbf{I2})$ | -4.1 | |
| **Step 7** | -7.9 | $\mathbf{2}_{\mathbf{C5}}(\mathbf{I3})$ | -7.8[a] | $\mathbf{2}_{\mathbf{C5}}(\mathbf{TS2})$ |
| **Step 8** | -7.8 | $\mathbf{2}_{\mathbf{C5}}(\mathbf{I4})$ | -7.8 | |
| **Step 9** | -9.0 | $\mathbf{2}_{\mathbf{C5}}^{+}(\mathbf{I5})$ | -9.0 | |
| **Step 10** | -12.5 | $\mathbf{2}_{\mathbf{C5}}(\mathbf{I5\text{-}R})$ | -5.2 | |
| **Step 11** | -5.2 | $\mathbf{2}_{\mathbf{C5}}(\mathbf{I6\text{-}R})$ | 1.5 | $\mathbf{2}_{\mathbf{C5}}(\mathbf{TS3})$ |
| **Step 12** | -4.7 | $\mathbf{2}_{\mathbf{C5}}(\mathbf{I7\text{-}R})$ | -4.7 | |
| **Step 13** | -10.1 | $\mathbf{2}_{\mathbf{C5}}^{+}(\mathbf{I8})$ | -10.1 | |

**Table S9.** $X_{TOF}$ of each intermediate and transition state using $\mathbf{2}_{\mathbf{C5}}^{+}$ for $CO_2$RR under an applied potential of Φ = −1.82 V versus the $Fc^{0/+}$ couple. The "degree of TOF control" for the TOF determining intermediate (TDI) and the TOF determining transition state (TDTS) based on the energy span model are highlighted in gray.

| | $X_{TOF}$, $I_j$ | | $X_{TOF}$, $T_i$ | |
|---|---|---|---|---|
| **Step 1** | 0.00 | $\mathbf{2}_{\mathbf{C5}}^{+}$ | 0.00 | |
| **Step 2** | 0.00 | $\mathbf{2}_{\mathbf{C5}}(\mathbf{red1\text{-}Br})$ | 0.00 | |
| **Step 3** | 0.00 | $\mathbf{2}_{\mathbf{C5}}^{+}(\mathbf{red1})$ | 0.00 | |
| **Step 4** | 0.93 | $\mathbf{2}_{\mathbf{C5}}(\mathbf{red2})$ | 0.00 | |
| **Step 5** | 0.00 | $\mathbf{2}_{\mathbf{C5}}(\mathbf{I1})$ | 0.74 | $\mathbf{2}_{\mathbf{C5}}(\mathbf{TS1})$ |
| **Step 6** | 0.00 | $\mathbf{2}_{\mathbf{C5}}(\mathbf{I2})$ | 0.00 | |
| **Step 7** | 0.00 | $\mathbf{2}_{\mathbf{C5}}(\mathbf{I3})$ | 0.00 | $\mathbf{2}_{\mathbf{C5}}(\mathbf{TS2})$ |
| **Step 8** | 0.00 | $\mathbf{2}_{\mathbf{C5}}(\mathbf{I4})$ | 0.00 | |
| **Step 9** | 0.00 | $\mathbf{2}_{\mathbf{C5}}^{+}(\mathbf{I5})$ | 0.00 | |
| **Step 10** | 0.07 | $\mathbf{2}_{\mathbf{C5}}(\mathbf{I5\text{-}R})$ | 0.00 | |
| **Step 11** | 0.00 | $\mathbf{2}_{\mathbf{C5}}(\mathbf{I6\text{-}R})$ | 0.26 | $\mathbf{2}_{\mathbf{C5}}(\mathbf{TS3})$ |
| **Step 12** | 0.00 | $\mathbf{2}_{\mathbf{C5}}(\mathbf{I7\text{-}R})$ | 0.00 | |
| **Step 13** | 0.00 | $\mathbf{2}_{\mathbf{C5}}^{+}(\mathbf{I8})$ | 0.00 | |

**Table S10.** Steps considered to calculate the TOF and $X_{TOF}$ using $\mathbf{2}_{\mathbf{C2}}^{+}$ for $CO_2RR$ under an applied potential of Φ = −1.82 V versus the $Fc^{0/+}$ couple. The TOF is calculated to be 1.0E+01 $s^{-1}$ at the ωB97X-D(SMD)/BS2//ωB97X-D(SMD)BS1 level of theory. The "degree of TOF control" ($X_{TOF}$) for the intermediates and transition states are given in Table S11. [a]The Gibbs free energy of the highest intermediate was employed for the transition state. The overall change in the Gibbs free energy is -4.2 kcal/mol. The TOF determining intermediate (TDI) and the TOF determining transition state (TDTS) based on the energy span model are highlighted in gray.

| | **Intermediates, $I_j$ (kcal/mol)** | | **Transition States, $T_i$ (kcal/mol)** | |
|---|---|---|---|---|
| **Step 1** | 0.0 | $\mathbf{2}_{\mathbf{C5}}^{+}$ | 0.0 | |
| **Step 2** | -3.9 | $\mathbf{2}_{\mathbf{C5}}(\mathbf{red1\text{-}Br})$ | -3.9 | |
| **Step 3** | -6.9 | $\mathbf{2}_{\mathbf{C5}}^{+}(\mathbf{red1})$ | -6.9 | |
| **Step 4** | -13.1 | $\mathbf{2}_{\mathbf{C5}}(\mathbf{red2})$ | -6.9 | |
| **Step 5** | -6.9 | $\mathbf{2}_{\mathbf{C2}}(\mathbf{I1})$ | 2.4 | $\mathbf{2}_{\mathbf{C2}}(\mathbf{TS1})$ |
| **Step 6** | -3.5 | $\mathbf{2}_{\mathbf{C2}}(\mathbf{I2})$ | -3.5 | |
| **Step 7** | -8.1 | $\mathbf{2}_{\mathbf{C2}}(\mathbf{I3})$ | -7.1[a] | $\mathbf{2}_{\mathbf{C2}}(\mathbf{TS2})$ |
| **Step 8** | -7.1 | $\mathbf{2}_{\mathbf{C2}}(\mathbf{I4})$ | -7.1 | |
| **Step 9** | -9.0 | $\mathbf{2}_{\mathbf{C5}}^{+}(\mathbf{I5})$ | -9.0 | |
| **Step 10** | -12.5 | $\mathbf{2}_{\mathbf{C5}}(\mathbf{I5\text{-}R})$ | -3.9 | |
| **Step 11** | -3.9 | $\mathbf{2}_{\mathbf{C2}}(\mathbf{I6\text{-}R})$ | 2.5 | $\mathbf{2}_{\mathbf{C2}}(\mathbf{TS3})$ |
| **Step 12** | -3.1 | $\mathbf{2}_{\mathbf{C2}}(\mathbf{I7\text{-}R})$ | -3.1 | |
| **Step 13** | -10.1 | $\mathbf{2}_{\mathbf{C5}}^{+}(\mathbf{I8})$ | -10.1 | |

**Table S11.** $X_{TOF}$ of each intermediate and transition state using $\mathbf{2}_{\mathbf{C2}}^{+}$ for $CO_2RR$ under an applied potential of Φ = −1.82 V versus the $Fc^{0/+}$ couple. The "degree of TOF control" for the TOF determining intermediate (TDI) and the TOF determining transition state (TDTS) based on the energy span model are highlighted in gray.

| | $X_{TOF}$, $I_j$ | | $X_{TOF}$, $T_i$ | |
|---|---|---|---|---|
| **Step 1** | 0.00 | $\mathbf{2}_{\mathbf{C5}}^{+}$ | 0.00 | |
| **Step 2** | 0.00 | $\mathbf{2}_{\mathbf{C5}}(\mathbf{red1\text{-}Br})$ | 0.00 | |
| **Step 3** | 0.00 | $\mathbf{2}_{\mathbf{C5}}^{+}(\mathbf{red1})$ | 0.00 | |
| **Step 4** | 0.83 | $\mathbf{2}_{\mathbf{C5}}(\mathbf{red2})$ | 0.00 | |
| **Step 5** | 0.00 | $\mathbf{2}_{\mathbf{C2}}(\mathbf{I1})$ | 0.38 | $\mathbf{2}_{\mathbf{C2}}(\mathbf{TS1})$ |
| **Step 6** | 0.00 | $\mathbf{2}_{\mathbf{C2}}(\mathbf{I2})$ | 0.00 | |
| **Step 7** | 0.00 | $\mathbf{2}_{\mathbf{C2}}(\mathbf{I3})$ | 0.00 | $\mathbf{2}_{\mathbf{C2}}(\mathbf{TS2})$ |
| **Step 8** | 0.00 | $\mathbf{2}_{\mathbf{C2}}(\mathbf{I4})$ | 0.00 | |
| **Step 9** | 0.00 | $\mathbf{2}_{\mathbf{C5}}^{+}(\mathbf{I5})$ | 0.00 | |
| **Step 10** | 0.16 | $\mathbf{2}_{\mathbf{C5}}(\mathbf{I5\text{-}R})$ | 0.00 | |
| **Step 11** | 0.00 | $\mathbf{2}_{\mathbf{C2}}(\mathbf{I6\text{-}R})$ | 0.62 | $\mathbf{2}_{\mathbf{C2}}(\mathbf{TS3})$ |
| **Step 12** | 0.00 | $\mathbf{2}_{\mathbf{C2}}(\mathbf{I7\text{-}R})$ | 0.00 | |
| **Step 13** | 0.00 | $\mathbf{2}_{\mathbf{C5}}^{+}(\mathbf{I8})$ | 0.00 | |

**Table S12.** Steps considered to calculate the TOF and $X_{TOF}$ using $\mathbf{3}_{\mathbf{C2}}^{+}$ for $CO_2RR$ under an applied potential of Φ = −1.82 V versus the $Fc^{0/+}$ couple. The TOF is calculated to be 1.6E+01 $s^{-1}$ at the ωB97X-D(SMD)/BS2//ωB97X-D(SMD)BS1 level of theory. The "degree of TOF control" ($X_{TOF}$) for the intermediates and transition states are given in Table S13. [a]The Gibbs free energy of the highest intermediate was employed for the transition state. The overall change in the Gibbs free energy is -4.2 kcal/mol. The TOF determining intermediate (TDI) and the TOF determining transition state (TDTS) based on the energy span model are highlighted in gray.

| | **Intermediates, $I_j$ (kcal/mol)** | | **Transition States, $T_i$ (kcal/mol)** | |
|---|---|---|---|---|
| **Step 1** | 0.0 | $\mathbf{3}_{\mathbf{C2}}^{+}$ | 0.0 | |
| **Step 2** | -4.6 | $\mathbf{3}_{\mathbf{C2}}(\mathbf{red1\text{-}Br})$ | -4.6 | |
| **Step 3** | -6.8 | $\mathbf{3}_{\mathbf{C2}}^{+}(\mathbf{red1})$ | -6.8 | |
| **Step 4** | -13.1 | $\mathbf{3}_{\mathbf{C2}}(\mathbf{red2})$ | -6.3 | |
| **Step 5** | -6.3 | $\mathbf{3}_{\mathbf{C2}}(\mathbf{I1})$ | 1.6 | $\mathbf{3}_{\mathbf{C2}}(\mathbf{TS1})$ |
| **Step 6** | -4.1 | $\mathbf{3}_{\mathbf{C2}}(\mathbf{I2})$ | -4.1 | |
| **Step 7** | -8.1 | $\mathbf{3}_{\mathbf{C2}}(\mathbf{I3})$ | -6.4[a] | $\mathbf{3}_{\mathbf{C2}}(\mathbf{TS2})$ |
| **Step 8** | -6.4 | $\mathbf{3}_{\mathbf{C2}}(\mathbf{I4})$ | -6.4 | |
| **Step 9** | -7.3 | $\mathbf{3}_{\mathbf{C2}}^{+}(\mathbf{I5})$ | -7.3 | |
| **Step 10** | -11.0 | $\mathbf{3}_{\mathbf{C2}}(\mathbf{I5\text{-}R})$ | -3.9 | |
| **Step 11** | -3.9 | $\mathbf{3}_{\mathbf{C2}}(\mathbf{I6\text{-}R})$ | 2.6 | $\mathbf{3}_{\mathbf{C2}}(\mathbf{TS3})$ |
| **Step 12** | -2.2 | $\mathbf{3}_{\mathbf{C2}}(\mathbf{I7\text{-}R})$ | -2.2 | |
| **Step 13** | -10.8 | $\mathbf{3}_{\mathbf{C2}}^{+}(\mathbf{I8})$ | -10.8 | |

**Table S13.** $X_{TOF}$ of each intermediate and transition state using $\mathbf{3}_{\mathbf{C2}}^{+}$ for $CO_2$RR under an applied potential of Φ = −1.82 V versus the $Fc^{0/+}$ couple. The "degree of TOF control" for the TOF determining intermediate (TDI) and the TOF determining transition state (TDTS) based on the energy span model are highlighted in gray.

| | $X_{TOF}$, $I_j$ | | $X_{TOF}$, $T_i$ | |
|---|---|---|---|---|
| **Step 1** | 0.00 | $\mathbf{3}_{\mathbf{C2}}^{+}$ | 0.00 | |
| **Step 2** | 0.00 | $\mathbf{3}_{\mathbf{C2}}(\mathbf{red1\text{-}Br})$ | 0.00 | |
| **Step 3** | 0.00 | $\mathbf{3}_{\mathbf{C2}}^{+}(\mathbf{red1})$ | 0.00 | |
| **Step 4** | 0.98 | $\mathbf{3}_{\mathbf{C2}}(\mathbf{red2})$ | 0.00 | |
| **Step 5** | 0.00 | $\mathbf{3}_{\mathbf{C2}}(\mathbf{I1})$ | 0.15 | $\mathbf{3}_{\mathbf{C2}}(\mathbf{TS1})$ |
| **Step 6** | 0.00 | $\mathbf{3}_{\mathbf{C2}}(\mathbf{I2})$ | 0.00 | |
| **Step 7** | 0.00 | $\mathbf{3}_{\mathbf{C2}}(\mathbf{I3})$ | 0.00 | $\mathbf{3}_{\mathbf{C2}}(\mathbf{TS2})$ |
| **Step 8** | 0.00 | $\mathbf{3}_{\mathbf{C2}}(\mathbf{I4})$ | 0.00 | |
| **Step 9** | 0.00 | $\mathbf{3}_{\mathbf{C2}}^{+}(\mathbf{I5})$ | 0.00 | |
| **Step 10** | 0.02 | $\mathbf{3}_{\mathbf{C2}}(\mathbf{I5\text{-}R})$ | 0.00 | |
| **Step 11** | 0.00 | $\mathbf{3}_{\mathbf{C2}}(\mathbf{I6\text{-}R})$ | 0.85 | $\mathbf{3}_{\mathbf{C2}}(\mathbf{TS3})$ |
| **Step 12** | 0.00 | $\mathbf{3}_{\mathbf{C2}}(\mathbf{I7\text{-}R})$ | 0.00 | |
| **Step 13** | 0.00 | $\mathbf{3}_{\mathbf{C2}}^{+}(\mathbf{I8})$ | 0.00 | |

**Table S14.** Steps considered to calculate the TOF and $X_{TOF}$ using $\mathbf{3}_{\mathbf{C5}}^{+}$ for $CO_2RR$ under an applied potential of Φ = −1.82 V versus the $Fc^{0/+}$ couple. The TOF is calculated to be 1.7E+01 $s^{-1}$ at the ωB97X-D(SMD)/BS2//ωB97X-D(SMD)BS1 level of theory. The "degree of TOF control" ($X_{TOF}$) for the intermediates and transition states are given in Table S15. [a]The Gibbs free energy of the highest intermediate was employed for the transition state. The overall change in the Gibbs free energy is -4.2 kcal/mol. The TOF determining intermediate (TDI) and the TOF determining transition state (TDTS) based on the energy span model are highlighted in gray.

| | **Intermediates, $I_j$ (kcal/mol)** | | **Transition States, $T_i$ (kcal/mol)** | |
|---|---|---|---|---|
| **Step 1** | 0.0 | $\mathbf{3}_{\mathbf{C2}}^{+}$ | 0.0 | |
| **Step 2** | -4.6 | $\mathbf{3}_{\mathbf{C2}}(\mathbf{red1\text{-}Br})$ | -4.6 | |
| **Step 3** | -6.8 | $\mathbf{3}_{\mathbf{C2}}^{+}(\mathbf{red1})$ | -6.8 | |
| **Step 4** | -13.1 | $\mathbf{3}_{\mathbf{C2}}(\mathbf{red2})$ | -7.5 | |
| **Step 5** | -7.5 | $\mathbf{3}_{\mathbf{C5}}(\mathbf{I1})$ | 1.3 | $\mathbf{3}_{\mathbf{C5}}(\mathbf{TS1})$ |
| **Step 6** | -2.5 | $\mathbf{3}_{\mathbf{C5}}(\mathbf{I2})$ | -2.5 | |
| **Step 7** | -7.7 | $\mathbf{3}_{\mathbf{C5}}(\mathbf{I3})$ | -6.5[a] | $\mathbf{3}_{\mathbf{C5}}(\mathbf{TS2})$ |
| **Step 8** | -6.5 | $\mathbf{3}_{\mathbf{C5}}(\mathbf{I4})$ | -6.5 | |
| **Step 9** | -7.3 | $\mathbf{3}_{\mathbf{C2}}^{+}(\mathbf{I5})$ | -7.3 | |
| **Step 10** | -11.0 | $\mathbf{3}_{\mathbf{C2}}(\mathbf{I5\text{-}R})$ | -3.8 | |
| **Step 11** | -3.8 | $\mathbf{3}_{\mathbf{C5}}(\mathbf{I6\text{-}R})$ | 2.6 | $\mathbf{3}_{\mathbf{C5}}(\mathbf{TS3})$ |
| **Step 12** | -1.4 | $\mathbf{3}_{\mathbf{C5}}(\mathbf{I7\text{-}R})$ | -1.4 | |
| **Step 13** | -10.8 | $\mathbf{3}_{\mathbf{C2}}^{+}(\mathbf{I8})$ | -10.8 | |

**Table S15.** $X_{TOF}$ of each intermediate and transition state using $\mathbf{3}_{\mathbf{C5}}^{+}$ for $CO_2RR$ under an applied potential of Φ = −1.82 V versus the $Fc^{0/+}$ couple. The "degree of TOF control" for the TOF determining intermediate (TDI) and the TOF determining transition state (TDTS) based on the energy span model are highlighted in gray.

| | $X_{TOF}$, $I_j$ | | $X_{TOF}$, $T_i$ | |
|---|---|---|---|---|
| **Step 1** | 0.00 | $\mathbf{3}_{\mathbf{C2}}^{+}$ | 0.00 | |
| **Step 2** | 0.00 | $\mathbf{3}_{\mathbf{C2}}(\mathbf{red1\text{-}Br})$ | 0.00 | |
| **Step 3** | 0.00 | $\mathbf{3}_{\mathbf{C2}}^{+}(\mathbf{red1})$ | 0.00 | |
| **Step 4** | 0.97 | $\mathbf{3}_{\mathbf{C2}}(\mathbf{red2})$ | 0.00 | |
| **Step 5** | 0.00 | $\mathbf{3}_{\mathbf{C5}}(\mathbf{I1})$ | 0.10 | $\mathbf{3}_{\mathbf{C5}}(\mathbf{TS1})$ |
| **Step 6** | 0.00 | $\mathbf{3}_{\mathbf{C5}}(\mathbf{I2})$ | 0.00 | |
| **Step 7** | 0.00 | $\mathbf{3}_{\mathbf{C5}}(\mathbf{I3})$ | 0.00 | $\mathbf{3}_{\mathbf{C5}}(\mathbf{TS2})$ |
| **Step 8** | 0.00 | $\mathbf{3}_{\mathbf{C5}}(\mathbf{I4})$ | 0.00 | |
| **Step 9** | 0.00 | $\mathbf{3}_{\mathbf{C2}}^{+}(\mathbf{I5})$ | 0.00 | |
| **Step 10** | 0.03 | $\mathbf{3}_{\mathbf{C2}}(\mathbf{I5\text{-}R})$ | 0.00 | |
| **Step 11** | 0.00 | $\mathbf{3}_{\mathbf{C5}}(\mathbf{I6\text{-}R})$ | 0.90 | $\mathbf{3}_{\mathbf{C5}}(\mathbf{TS3})$ |
| **Step 12** | 0.00 | $\mathbf{3}_{\mathbf{C5}}(\mathbf{I7\text{-}R})$ | 0.00 | |
| **Step 13** | 0.00 | $\mathbf{3}_{\mathbf{C2}}^{+}(\mathbf{I8})$ | 0.00 | |

**2.5. Second-order perturbation analyses.**

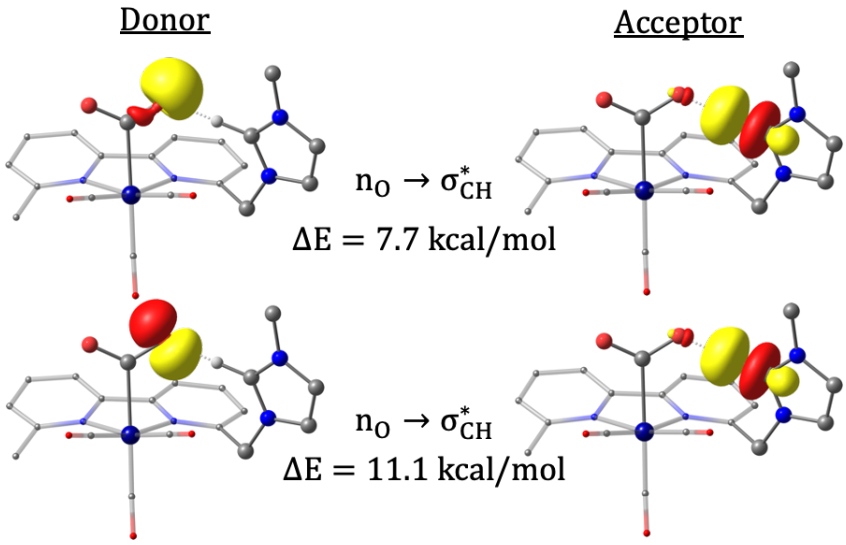


**Figure S18.** Isosurface (0.07 au) plots of the principal second-order perturbation interactions between carbon dioxide and the C2-H group of the imidazolium ligand in $\mathbf{1_{C2}(I2)}$. Non-participating hydrogen atoms are omitted for clarity. All reported contributions were obtained from the alpha spin orbitals.

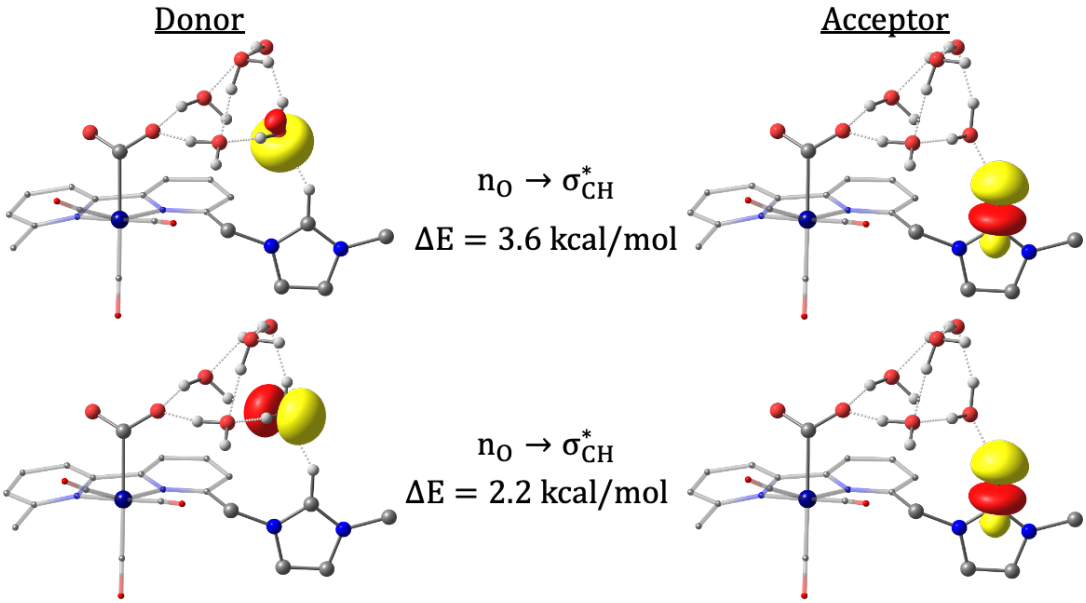


**Figure S19.** Isosurface (0.07 au) plots of the principal second-order perturbation interactions between the water cluster and the C2-H group of the imidazolium ligand in $\mathbf{1_{C2}(I3)}$. Non-participating hydrogen atoms are omitted for clarity. All reported contributions were obtained from the alpha spin orbitals.

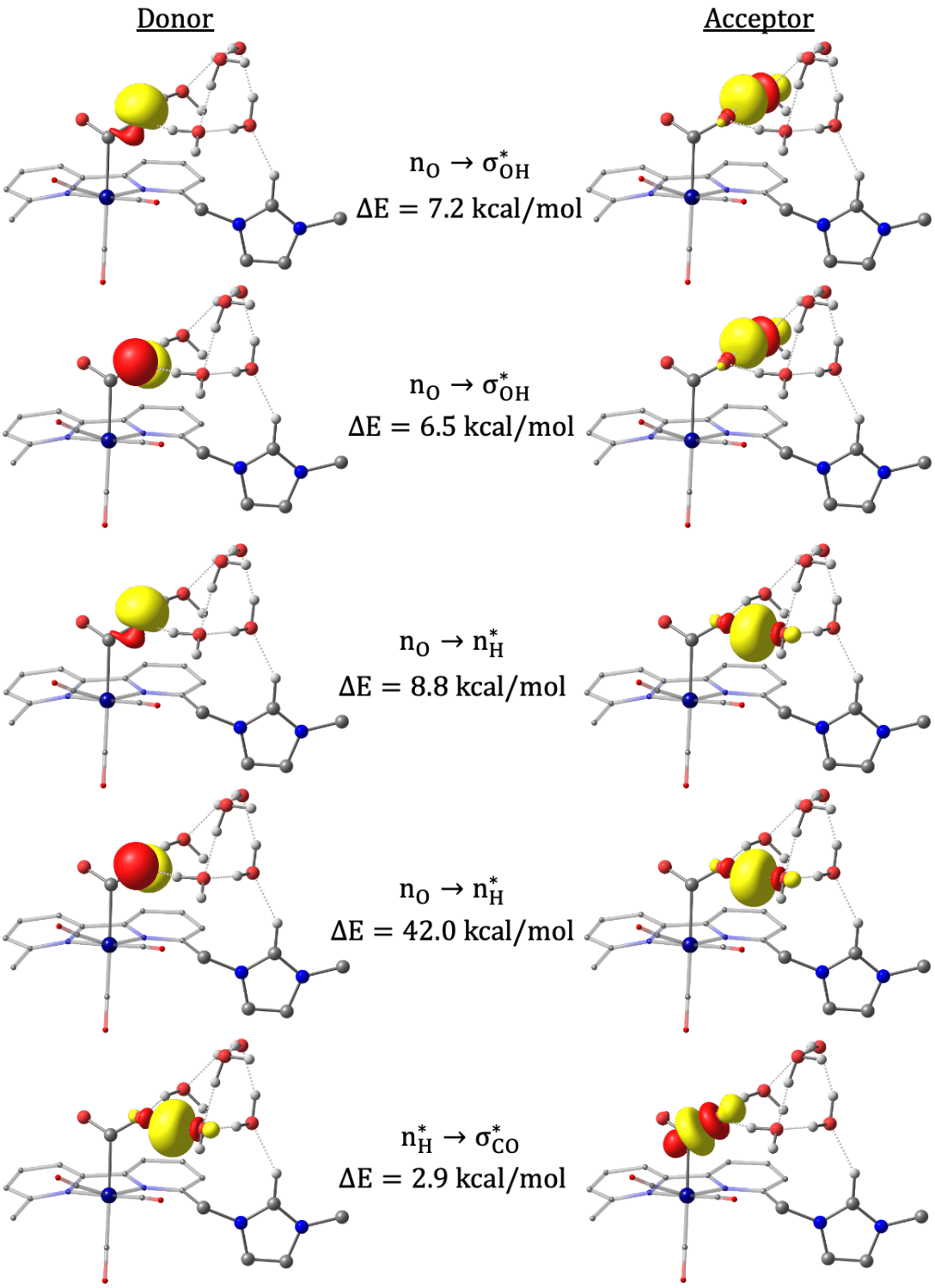


**Figure S20.** Isosurface (0.07 au) plots of the principal second-order perturbation interactions between the water cluster and $CO_2$ in $\mathbf{1}_{\mathbf{C2}}(\mathbf{I3})$. Non-participating hydrogen atoms are omitted for clarity. All reported contributions were obtained from the alpha spin orbitals.

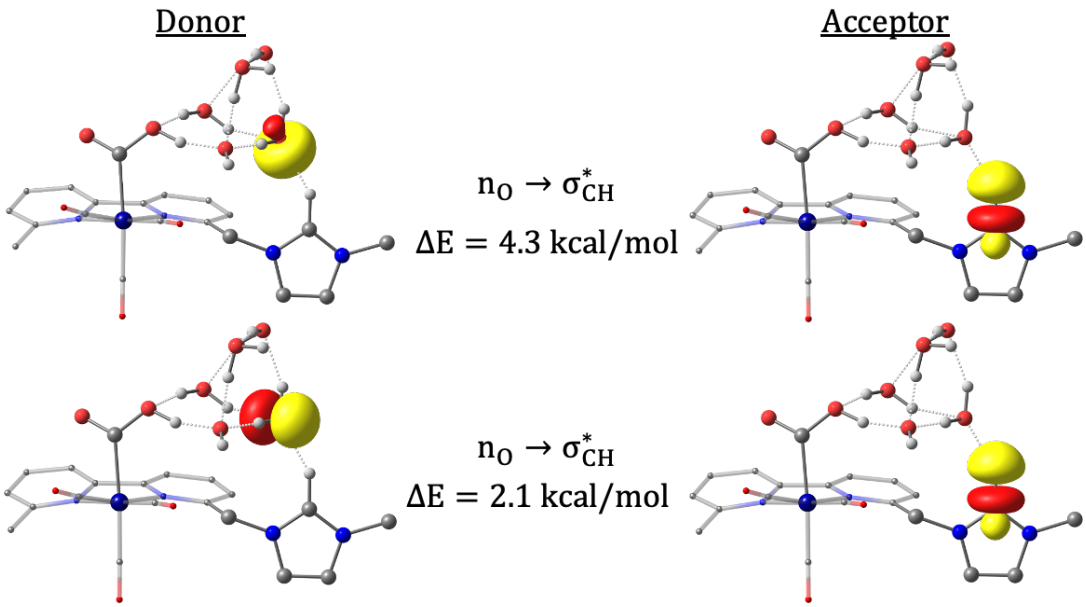


**Figure S21.** Isosurface (0.07 au) plots of the principal second-order perturbation interactions between the water cluster and the C2-H group of the imidazolium ligand in $\mathbf{1_{C2}(I4)}$. Non-participating hydrogen atoms are omitted for clarity. All reported contributions were obtained from the alpha spin orbitals.

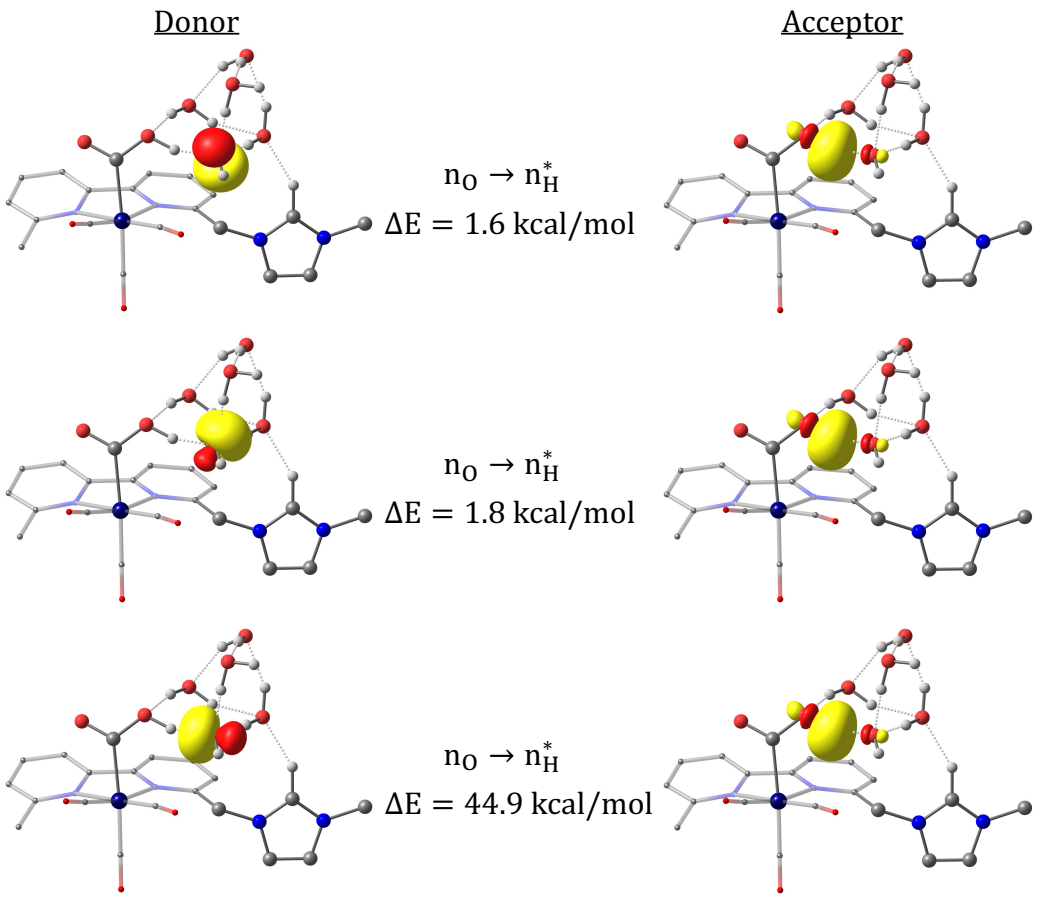


**Figure S22.** Isosurface (0.07 au) plots of the principal second-order perturbation interactions between the hydroxide anion and the carboxyl group in $\mathbf{1}_{\mathbf{C2}}(\mathbf{I4})$. Non-participating hydrogen atoms are omitted for clarity. All reported contributions were obtained from the alpha spin orbitals.

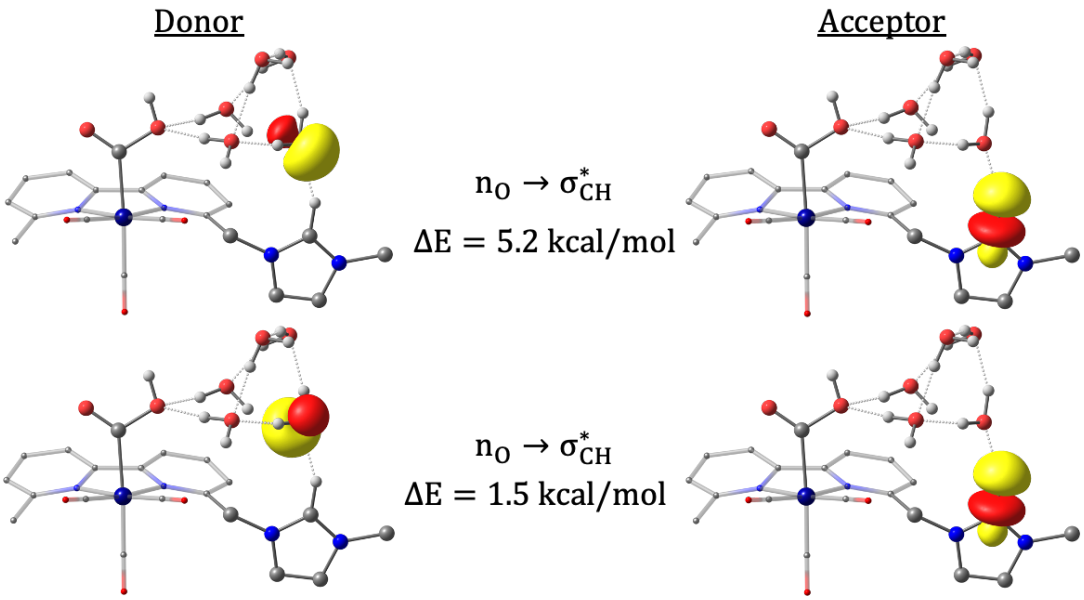


**Figure S23.** Isosurface (0.07 au) plots of the principal second-order perturbation interactions between the water cluster and the C2-H group of the imidazolium ligand in $\mathbf{1}_{\mathbf{C2}}(\mathbf{I6\text{-}R})$. Non-participating hydrogen atoms are omitted for clarity. All reported contributions were obtained from the alpha spin orbitals.

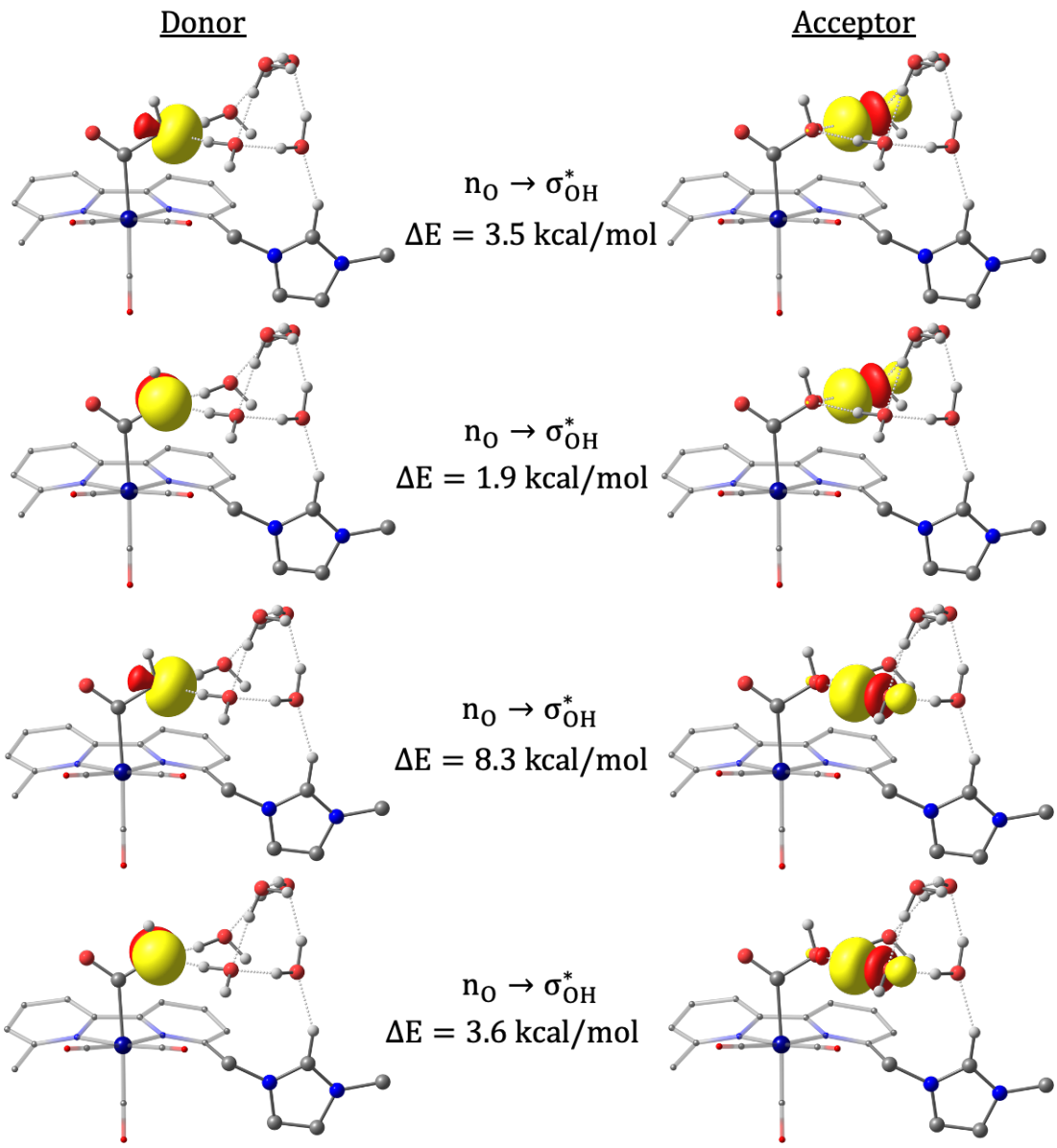


**Figure S24.** Isosurface (0.07 au) plots of the principal second-order perturbation interactions between the water cluster and the carboxyl group in $\mathbf{1}_{\mathbf{C2}}(\mathbf{I6\text{-}R})$. Non-participating hydrogen atoms are omitted for clarity. All reported contributions were obtained from the alpha spin orbitals.

**Table S16.** Principal second-order perturbation interaction energies (kcal/mol) between $CO_2$ and the substituent on the imidazolium group for the metallocarboxylate intermediates (i.e., contribution above 1.00 kcal/mol threshold). [a]This intermolecular interaction is obtained from a hydrogen-bonding interaction between the methylene bridge and $CO_2$. All reported contributions were obtained from the alpha spin orbitals.

| Species | $n_O \rightarrow \sigma^*_{CH}$ | | |
|---|---|---|---|
| $\mathbf{1_{C2}(I2)}$ | 11.09 | 7.73 | |
| $\mathbf{1_{C5}(I2)}$ | 6.13 | 4.51 | |
| $\mathbf{2_{C2}(I2)}$ | 2.12 | 2.11 | |
| | 3.67[a] | 3.57[a] | |
| $\mathbf{2_{C5}(I2)}$ | 5.39 | 3.68 | |
| $\mathbf{3_{C2}(I2)}$ | 2.08 | 1.45 | |
| | 2.07[a] | 1.37[a] | 1.04[a] |
| $\mathbf{3_{C5}(I2)}$ | 1.32[a] | | |

**Table S17.** Principal second-order perturbation interaction energies (kcal/mol) between the water cluster and the substituent on the imidazolium ligand for the transition states corresponding to the formation of the metallocarboxylic acid intermediates (i.e., contribution above 0.50 kcal/mol threshold). All reported contributions were obtained from the alpha spin orbitals.

| Species | $n_O \rightarrow \sigma^*_{CH}$ | |
|---|---|---|
| $\mathbf{1_{C2}(TS2)}$ | 3.33 | 2.31 |
| $\mathbf{1_{C5}(TS2)}$ | 3.44 | 1.20 |
| $\mathbf{2_{C2}(TS2)}$ | 1.57 | 1.37 |
| $\mathbf{2_{C5}(TS2)}$ | 2.92 | 0.94 |
| $\mathbf{3_{C2}(TS2)}$ | 1.44 | 1.35 |
| $\mathbf{3_{C5}(TS2)}$ | 1.20 | 0.95 |

**Table S18.** Principal second-order perturbation interaction energies (kcal/mol) between the water cluster and the substituent on the imidazolium ligand for the C-O bond cleavage transition states along the reduction-first pathway (i.e., contribution above 0.50 kcal/mol threshold). All reported contributions were obtained from the alpha spin orbitals.

| Species | $n_O \rightarrow \sigma^*_{CH}$ | |
|---|---|---|
| $\mathbf{1}_{C2}(\mathbf{TS3})$ | 6.37 | 0.99 |
| $\mathbf{1}_{C5}(\mathbf{TS3})$ | 4.96 | |
| $\mathbf{2}_{C2}(\mathbf{TS3})$ | 1.40 | 1.35 |
| $\mathbf{2}_{C5}(\mathbf{TS3})$ | 4.49 | |
| $\mathbf{3}_{C2}(\mathbf{TS3})$ | 1.60 | 0.94 |
| $\mathbf{3}_{C5}(\mathbf{TS3})$ | 0.94 | 0.82 |

**3. References.**


1. A. V. Marenich, C. J. Cramer and D. G. Truhlar, *Journal of Physical Chemistry B*, 2009, **113**, 6378-6396.
2. S. Grimme, *Chem. Eur. J.*, 2012, **18**, 9955-9964.
3. S. Sung, X. Li, L. M. Wolf, J. R. Meeder, N. S. Bhuvanesh, K. A. Grice, J. A. Panetier and M. Nippe, *J. Am. Chem. Soc.*, 2019, **141**, 6569-6582.
4. E. D. Glendening, A. E. Reed, J. E. Carpenter and F. Weinhold, *NBO Version 3.1*, Theoretical Chemistry Institute, University of Wisconsin, Madison, WI, 1990.
5. M. J. Frisch, G. W. Trucks, H. B. Schlegel, G. E. Scuseria, M. A. Robb, J. R. Cheeseman, G. Scalmani, V. Barone, G. A. Petersson, H. Nakatsuji, X. Li, M. Caricato, A. Marenich, J. Bloino, B. G. Janesko, R. Gomperts, B. Mennucci, H. P. Hratchian, J. V. Ortiz, A. F. Izmaylov, J. L. Sonnenberg, D. Williams-Young, F. Ding, F. Lipparini, F. Egidi, J. Goings, B. Peng, A. Petrone, T. Henderson, D. Ranasinghe, V. G. Zakrzewski, J. Gao, N. Rega, G. Zheng, W. Liang, M. Hada, M. Ehara, K. Toyota, R. Fukuda, J. Hasegawa, M. Ishida, T. Nakajima, Y. Honda, O. Kitao, H. Nakai, T. Vreven, K. Throssell, J. J. A. Montgomery, J. E. Peralta, F. Ogliaro, M. Bearpark, J. J. Heyd, E. Brothers, K. N. Kudin, V. N. Staroverov, T. Keith, R. Kobayashi, J. Normand, K. Raghavachari, A. Rendell, J. C. Burant, S. S. Iyengar, J. Tomasi, M. Cossi, J. M. Millam, M. Klene, C. Adamo, R. Cammi, J. W. Ochterski, R. L. Martin, K. Morokuma, O. Farkas, J. B. Foresman and D. J. Fox, *Gaussian 09, Revision E.01*, Gaussian, Inc., Wallingford CT, 2009.